



Mitochondrial aspartate regulates TNF biogenesis and autoimmune tissue inflammation

Bowen Wu¹, Tuantuan V. Zhao¹, Ke Jin¹, Zhaolan Hu¹, Matthew P. Abdel², Ken J. Warrington¹, Jörg J. Goronzy^{1,3} and Cornelia M. Weyand^{1,3}✉

Misdirected immunity gives rise to the autoimmune tissue inflammation of rheumatoid arthritis, in which excess production of the cytokine tumor necrosis factor (TNF) is a central pathogenic event. Mechanisms underlying the breakdown of self-tolerance are unclear, but T cells in the arthritic joint have a distinctive metabolic signature of ATP^{lo} acetyl-CoA^{hi} proinflammatory effector cells. Here we show that a deficiency in the production of mitochondrial aspartate is an important abnormality in these autoimmune T cells. Shortage of mitochondrial aspartate disrupted the regeneration of the metabolic cofactor nicotinamide adenine dinucleotide, causing ADP deribosylation of the endoplasmic reticulum (ER) sensor GRP78/BiP. As a result, ribosome-rich ER membranes expanded, promoting co-translational translocation and enhanced biogenesis of transmembrane TNF. ER^{rich} T cells were the predominant TNF producers in the arthritic joint. Transfer of intact mitochondria into T cells, as well as supplementation of exogenous aspartate, rescued the mitochondria-instructed expansion of ER membranes and suppressed TNF release and rheumatoid tissue inflammation.

Rheumatoid arthritis (RA) is a classic autoimmune disease with a decade-long preclinical phase during which patients lose self-tolerance and begin to produce autoantibodies against post-translationally modified proteins¹. During clinically apparent RA, innate and adaptive immune cells infiltrate into the synovial membrane and, together with joint-endogenous cells, form a tissue-destructive pannus. TNF functions as a critical cytokine in RA pathogenesis and TNF inhibitors have fundamentally reshaped the therapeutic landscape of RA^{2,3}. TNF is mostly considered to be an innate cytokine, but recent single-cell transcriptomics of synovial cells have assigned the highest *TNF* transcripts to T cells⁴. Pathomechanisms leading to aberrant TNF production are unknown, necessitating current anti-TNF therapies to rely exclusively on blocking the secreted cytokine. Lack and loss of efficacy and adverse effects have raised the demand for more precise targeting of inappropriate TNF secretion⁵. Also, the promise of early immune modulation in at-risk individuals before clinical disease requires molecular definition of underlying processes.

Cell type-specific, TNF knockout mouse models have demonstrated distinct and nonredundant functions of T cell- and macrophage-derived TNF, both in anti-bacterial immunity and in induction of autoimmunity⁶. TNF-producing type 1 helper T cell expansion in both blood and liver are typical for patients with autoimmune hepatitis⁷. Activated T cells, via the release of TNF, instruct myeloid cells to produce inflammasome-independent interleukin (IL)-1 β to cause autoimmunity⁸. A distinct tissue-resident population of TNF-producing CD4⁺ T cells promotes mucosal development and mediates inflammation in necrotizing enterocolitis⁹. In RA, T cells are important pathogenic drivers required for very early, intermediate and late stages of the disease process^{10,11}. Required for autoantibody production, these cells also sustain synoviocyte proliferation, tissue inflammation, neoangiogenesis and cartilage and bone erosion^{10,12}. In mature synovitis, T cells are one of the most abundant cell types, comprising 30–50% of synovial tissue cells¹³. T cell-directed TNF overexpression is sufficient to promote arthritis,

wasting syndrome and organ necrosis¹⁴. In patients with RA, naive CD4⁺ T cells are imprinted with a metabolic signature that biases their differentiation into short-lived effector T cells (SLECs) instead of long-lived memory precursors¹⁵. Important elements of the metabolic program are a slowdown in glycolysis and glucose shunting to the biosynthetic pentose phosphate pathway, facilitated by a shift in the *PFKFB3:G6PD* expression ratio^{16,17}. A major abnormality is the transcriptional repression of *SUCLG2*, an enzyme central to the mitochondrial tricarboxylic acid (TCA) cycle¹⁸. Unable to convert 2-oxoglutarate (2-OG) into succinate and impaired in oxidative phosphorylation, RA T cells reverse the TCA cycle and accumulate acetyl-CoA. Together with surplus reduced nicotinamide adenine dinucleotide phosphate (NADPH) production and a reductive environment, acetyl-CoA oversupply expedites lipogenesis and membrane formation, supporting the differentiation of tissue-invasive T cells^{16,18,19}. Defects in mitochondrial DNA repair²⁰, as well as misrouting of 5'-AMP-activated protein kinase away from the lysosomal surface²¹, sustain the defect in mitochondrial fitness and enable persistent mammalian target of rapamycin activation, promoting differentiation into SLECs despite the lack of ATP.

In the present study, we show that the T cell disposition for membrane expansion extends to the endomembrane system and supports growth of the ER, where it affects the biogenesis of transmembrane TNF. Mitochondrial insufficiency in RA T cells was coupled with enlargement of ER membranes. Specifically, lack of mitochondrial aspartate production prevented cytosolic oxidized nicotinamide adenine dinucleotide (NAD⁺) regeneration, causing deribosylation of the ER stress sensor GRP78/BiP and dissociation from the kinase/endoribonuclease inositol-requiring enzyme 1 α (IRE1 α). The resulting expansion of ribosome-rich ER membranes enhanced post-translational translocation of the type II transmembrane protein TNF, turning RA T cells into TNF superproducers. Transfer of intact mitochondria into T cells or aspartate supplementation suppressed TNF production and treated synovial tissue inflammation. These data connect autoimmune tissue

¹Department of Medicine, Mayo Clinic College of Medicine and Science, Rochester, MN, USA. ²Department of Orthopedic Surgery, Mayo Clinic College of Medicine and Science, Rochester, MN, USA. ³School of Medicine, Stanford University, Stanford, CA, USA. ✉e-mail: cweyand@stanford.edu

inflammation to dysfunctional interorganelle communication and define mitochondrial intactness in T cells as an important component of tissue tolerance.

Results

Mitochondrial insufficiency promotes ER expansion. Naive CD4⁺ T cells from patients with RA have a mitochondrial defect, manifesting with low oxygen consumption and low mitochondrial membrane potential (MMP) (Fig. 1a–c), whereas mitochondrial mass is similar between healthy and RA T cells (Extended Data Fig. 1). To understand how the lack of mitochondrial fitness impacts other organelles, we quantified ER mass. Flow cytometry for ER-positioned, ATP-sensitive K⁺ channels (marked by ER Tracker) and confocal imaging for the ER-resident enzyme protein disulfide isomerase (PDI) revealed an inverse relationship between the MMP and the biomass of the ER (Fig. 1d,e). Cell size-restricted gating (Extended Data Fig. 2) confirmed the negative correlation between MMP and ER Tracker intensity in all subpopulations (Fig. 1f). Compared with healthy T cells, CD4⁺ T cells from patients with RA had a higher ER Tracker signal (Fig. 1g) and expressed more of the ER chaperone calnexin (Fig. 1h,i). By contrast, ER Tracker signals in activated CD4⁺ T cells from patients with psoriatic arthritis (PsA) were indistinguishable from age-matched controls (Fig. 1j), indicating that the expansion of ER size is not simply a consequence of systemic inflammation. RA T cells synthesized significantly more phosphatidylcholine, one of the major phospholipids needed for biomembrane generation (Fig. 1k). Transmission electron microscopy confirmed highly abundant and elongated ER structures in activated CD4⁺ T cells from patients with RA (Fig. 1l).

ER biogenesis and expansion are partially controlled by ER stress-related signals^{22,23}. We therefore explored whether ER stress contributes to the ER^{rich} phenotype of RA T cells. When activated, naive CD4⁺ T cells from patients with RA disproportionately upregulated the ER stress gene signature (Fig. 2a). We verified that ER stress promotes expansion of the ER membrane system by overexpressing the active form of XBP1 (XBP1S) in healthy T cells and quantifying ER biomass (Extended Data Fig. 3a–e). To address whether immunomodulatory treatment could affect ER biogenesis, we compared expression level of XBP1S in patients with or without methotrexate treatment; no significant difference was observed in these two patient cohorts (Extended Data Fig. 3f). To define whether mitochondrial activity regulates ER stress signaling, T cells were sorted into MMP^{lo} and MMP^{hi} subpopulations (Fig. 2b). ER stress gene expression was a feature of T cells with low mitochondrial activity (Fig. 2c). Distinct to RA T cells, PsA-derived T cells did not have abnormal ER stress signals (Fig. 2d).

To examine whether mitochondria-derived signals determine ER size and function, we quantified ER-associated membranes after inhibiting the electron transport chain complex I with rotenone (10 nM). Impaired electron transport prompted an increase in ER mass (Fig. 2e). Other mitochondrial respiration inhibitors (pieridin A, antimycin A, oligomycin) had similar effects (Extended Data Fig. 4). To repair defective mitochondria in RA T cells, exogenous mitochondria were harvested and transferred into RA recipient cells (Extended Data Fig. 5a). Mitochondrial transfer at a donor:recipient cell ratio of 10:1 yielded excellent improvement in MMP (Extended Data Fig. 5b,c). Delivery of exogenous mitochondria from healthy T cells into RA T cells restored the MMP to normal levels (Fig. 2f) and suppressed ER biomass by 30% (Fig. 2g). Mitochondria harvested from RA T cells failed to restore the ER size.

These data identify mitochondrial metabolism as a regulator of ER biogenesis and classify CD4⁺ T cells from patients with RA as MMP^{lo} ER^{rich}.

Mitochondria-derived aspartate controls ER size. The fact that supplying healthy mitochondria corrected the inappropriate

expansion of ER membranes in RA T cells directed attention to mitochondria–ER interorganelle communication. Metabolites of mitochondrial origin have been recognized as signal carriers controlling different cellular functions^{24,25}. In previous work, we described a shift in the 2-oxoglutarate (2-OG):succinate ratio as a distinguishing feature of RA T cells, imposed by disruption of the TCA cycle¹⁸. To address which mitochondrial signals restrain ER expansion and clarify how the ER senses impaired mitochondrial fitness, we screened mitochondrial intermediates. Exogenous 2-OG left ER mass unaffected (Fig. 3a), whereas succinate, malate and, more so, oxaloacetate and aspartate rapidly suppressed formation of ER membranes in RA T cells (Fig. 3a). Aspartate is synthesized in the mitochondrial matrix from malate–oxaloacetate by the transaminase glutamic–oxaloacetic transaminase 2 (GOT2) and then it is transported into the cytosol. Under conditions of NADH availability, cytosolic aspartate is converted back into malate to re-enter the mitochondria through the malate–aspartate shuttle (Fig. 3b). Activation of healthy T cells resulted in accumulation of aspartate (4 nmol per 10⁶ cells), whereas RA T cells generated <2.5 nmol per 10⁶ cells (Fig. 3c). Similarly, RA T cells lagged behind in producing adequate concentrations of oxaloacetate, the precursor of aspartate in the TCA cycle (Fig. 3d). The aspartate^{lo} phenotype was not due to insufficient glutamic–oxaloacetic transaminases; *GOT1* and *GOT2* transcript concentrations were indistinguishable in healthy and RA T cells (Extended Data Fig. 6). Exogenous aspartate corrected the ER stress gene signature (Fig. 2e) and inhibited the inappropriate biosynthesis of phosphatidylcholine, a membrane-building precursor required for ER biomass generation (Fig. 3f). Maintenance of cellular aspartate concentrations required intactness of mitochondrial metabolism. Inhibiting mitochondrial respiration through the complex I inhibitor rotenone dramatically decreased aspartate levels in healthy T cells (Fig. 3g), whereas the transfer of healthy mitochondria into RA T cells restored aspartate generation (Fig. 3h). Knockdown of GOT2, the gate-keeper enzyme in aspartate synthesis, successfully mimicked the aspartate^{lo} phenotype of RA T cells (Fig. 3i), and healthy T cells responded to GOT2 loss of function with increased formation of ER membranes and upregulation of the ER stress gene signature (Fig. 3j,k). Exogenous aspartate rescued the ER expansion induced by GOT2 knockdown (Fig. 3j).

These data identify the amino acid aspartate as a sensitive biomarker of mitochondrial respiration and as a signal transducer between mitochondria and the ER membrane system.

Aspartate supplementation suppresses tissue inflammation. To test whether the aspartate^{lo} phenotype in RA T cells is disease relevant and whether supplementation of aspartate can protect tissue from inflammatory damage, we induced synovitis in human synovium-engrafted NSG (NOD scid gamma) mice and treated the chimeras with aspartate. RA peripheral blood mononuclear cells (PBMCs) induced robust synovitis, which was successfully suppressed by aspartate treatment (Fig. 4a). Transcriptomic analysis of the tissue lesions revealed a marked beneficial effect of aspartate supplementation lowering T cell receptor (*TRB*) expression and curtailing *TBX21* and *RORG* messenger RNA accrual (Fig. 4b). Immunohistochemical analysis confirmed that the frequency of tissue-residing CD3⁺ interferon (IFN)- γ ⁺ T cells was highly dependent on aspartate availability, declining by 65% with aspartate supplementation (Fig. 4c). The mRNA levels for the inflammatory mediators IFN- γ , IL-17, IL-6, TNF and IL-1 β all decreased (Fig. 4d), indicating successful containment of tissue inflammation. Conversely, the anti-inflammatory genes *TGFB* and *IL10* were not affected.

Together, these data identify the mitochondrial intermediate aspartate as a regulator of ER mass and an anti-inflammatory mediator.

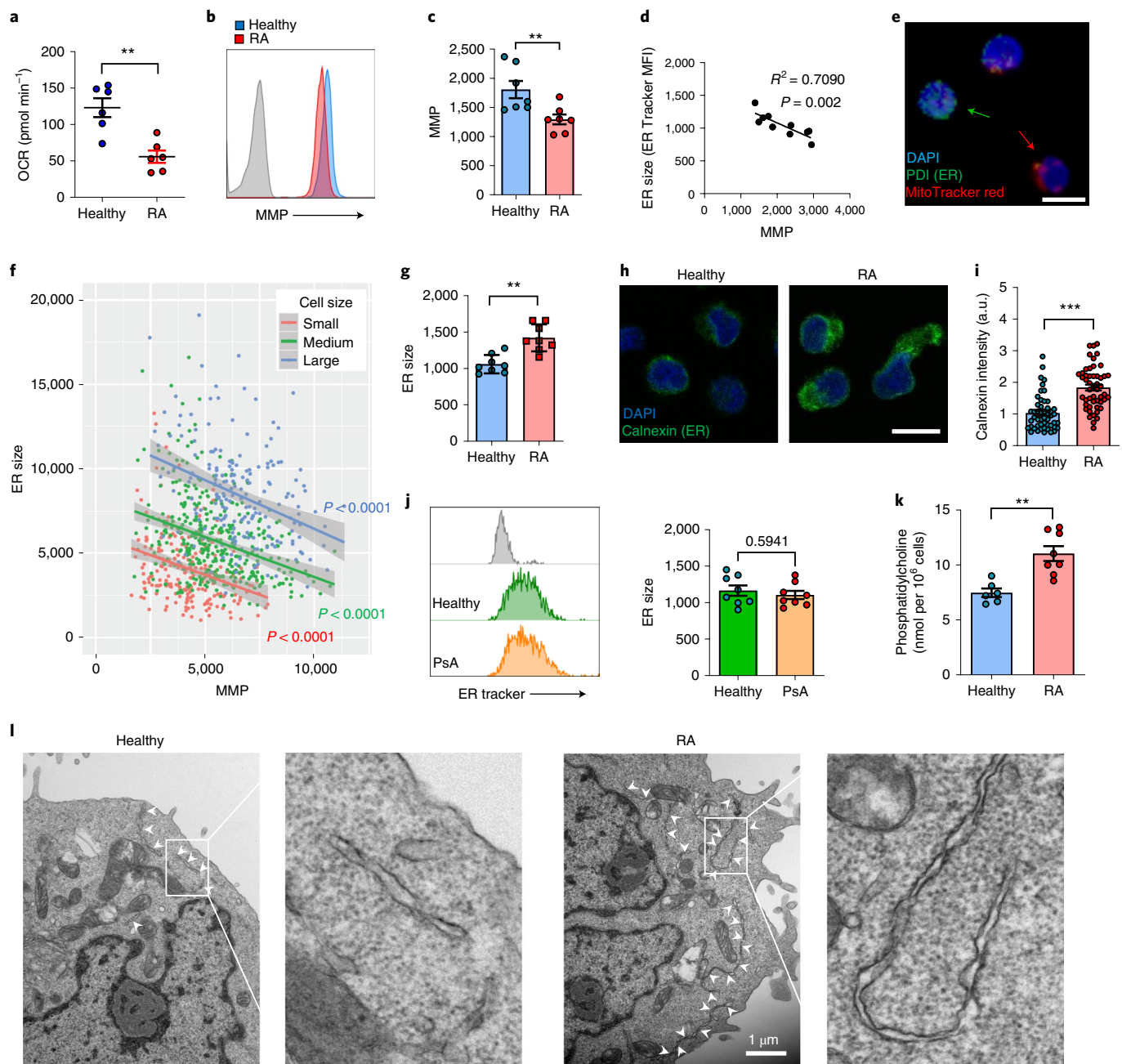


Fig. 1 | Mitochondrial insufficiency and ER expansion in RA. Naive CD4⁺CD45RA⁺ T cells from patients with RA or PsA and age-matched healthy individuals were stimulated for 72 h. **a–c**, Reduced mitochondrial fitness in RA T cells. **a**, Basal mitochondrial oxygen consumption rates (OCR) measured by Seahorse Analyzer ($n=6$ each). **b,c**, MMP by flow cytometry (MitoTrackerRed). Representative histogram (**b**) and summary data (**c**; $n=7$ each). **d**, Correlation of ER size (ER Tracker median of fluorescence intensity (MFI)) and mitochondrial membrane potential in healthy T cells by linear regression ($n=10$). **e**, Representative confocal microscopy imaging of the ER enzyme PDI and MMP (MitoTrackerRed) from three independent experiments. The green arrow marks a cell with abundant ER and the red arrow marks a cell with high mitochondrial activity. Scale bar, 10 μm . **f**, Correlation of ER size (ER Tracker intensity) and MMP in cells gated based on cell size. Linear regression with confidence interval shown in gray around the regression line. **g–i**, Expanded ER size in RA T cells. **g**, Flow cytometric quantification of ER size (ER Tracker MFI) in RA and healthy control T cells ($n=8$ each). **h,i**, Confocal microscopy imaging of the ER chaperone protein calnexin in RA and healthy T cells. Representative images (**h**). Scale bar, 10 μm . Single-cell calnexin intensity quantification (**i**; $n=50$ T cells from 5 healthy and 5 RA samples). a.u., arbitrary units. **j**, Flow cytometric quantification of ER size in T cells from patients with PsA and healthy donors ($n=8$ each). **k**, Intracellular phosphatidylcholine concentrations in healthy and RA T cells (healthy: $n=6$; RA: $n=8$). **l**, Representative transmission electron microscope image of healthy and RA T cells from 30 cells from 3 healthy and 3 RA samples. The white arrows indicate ER. Scale bar, 1 μm . All data are mean \pm s.e.m. Two-tailed, unpaired Mann–Whitney–Wilcoxon rank test (**a,c,g–k**): * $P < 0.05$, ** $P < 0.01$, *** $P < 0.001$.

Aspartate regulates BiP ADP ribosylation. The malate–aspartate shuttle functions primarily to translocate electrons produced during glycolysis into the mitochondria for oxidative phosphory-

lation²⁶. Essentially, aspartate is dispatched from mitochondria as an electron acceptor, facilitating the cytoplasmic regeneration of NAD⁺ from NADH, and then malate re-enters the mitochondria

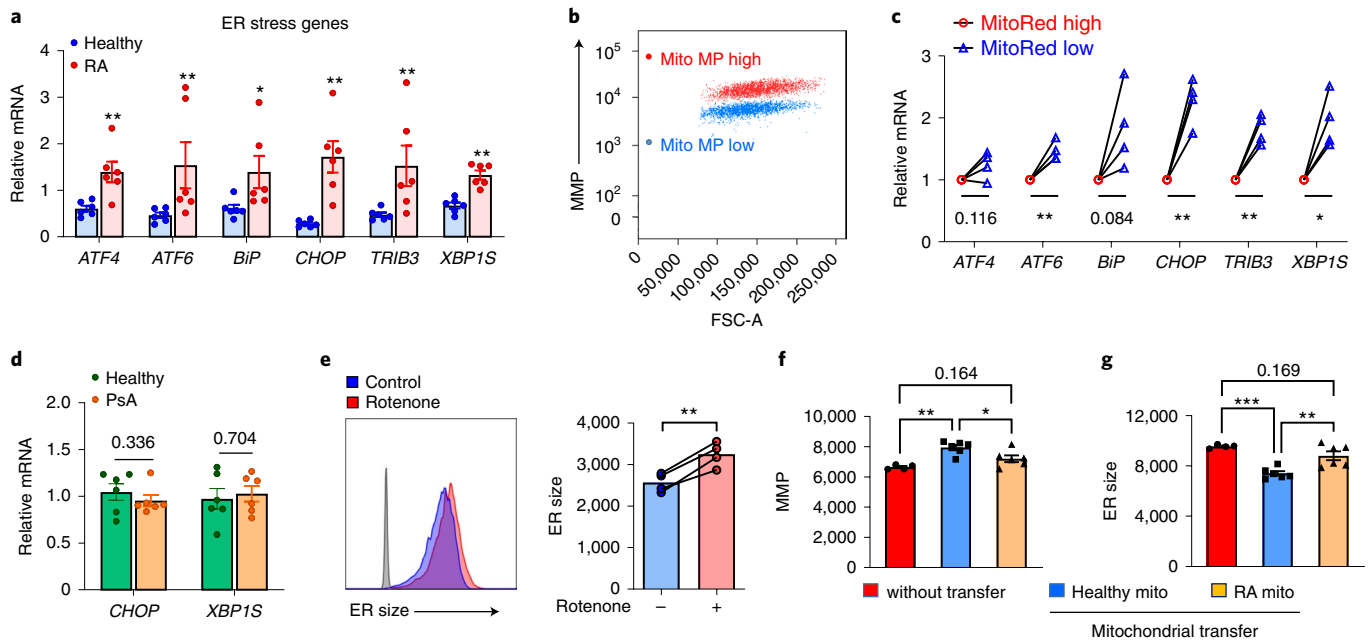


Fig. 2 | Mitochondrial insufficiency promotes ER expansion. **a**, ER stress gene expression (qPCR) in healthy and RA T cells (healthy: $n=6$; RA: $n=6$). **b,c**, Separation of two CD4⁺ T cell subpopulations based on MMP. Representative scatter plots (**b**). qPCR analysis of ER stress genes in Mito MP^{hi} and Mito MP^{lo} T cells (**c**; $n=4$). **d**, Comparison of *CHOP* and *XBP1S* mRNA levels in healthy and PsA T cells ($n=6$). **e**, Mitochondrial stress expands ER size. Healthy naive T cells were activated for 72 h with or without the complex I inhibitor rotenone (10 nM). Histogram of ER Tracker staining and collective MFI ($n=4$). **f,g**, Mitochondrial transfer corrects ER size. CD4⁺CD45RA⁺ T cells from patients with RA were stimulated with anti-CD3/CD28 for 48 h. The mitochondria isolated from healthy or RA CD4⁺ T cells were transferred into RA T cells (donor cell number/recipient cell number = 10:1). MMP (**f**) and ER size (**g**) in RA T cells after mitochondria (mito) transfer ($n=6$). All data are mean \pm s.e.m. Two-tailed, unpaired Mann-Whitney-Wilcoxon rank test (**a,d**); two-tailed, paired Student's *t*-test (**c,e**); one-way ANOVA and post-ANOVA, pair-wise, two-group comparisons conducted with Tukey's method (**f,g**): * $P < 0.05$, ** $P < 0.01$, *** $P < 0.001$.

as an electron carrier (Fig. 3b). To test whether NAD⁺ and NADH concentrations are affected by aspartate shortage, we measured intracellular NAD⁺:NADH in healthy and patient-derived CD4⁺ T cells. Healthy T cells reached NAD⁺ levels of 550 pmol per 10⁶ cells and NADH concentrations of 70 pmol per 10⁶ cells, resulting in a NAD⁺:NADH ratio >7 . With reduced NAD⁺ and elevated NADH, RA T cells achieved a NAD⁺:NADH ratio of just 3 (Fig. 5a–c). Treatment with aspartate or transfer of exogenous mitochondria significantly improved NAD⁺ regeneration (Fig. 5d,e). Inhibition of mitochondrial respiration with the complex I inhibitor rotenone essentially prevented conversion of NADH into NAD⁺ (Fig. 5f), implicating aspartate and mitochondrial intactness in maintaining the NAD⁺:NADH balance. To examine whether NAD⁺ functions similarly to aspartate in regulating ER mass/function, RA T cells were activated with or without a NAD⁺ supplement. Similar to aspartate, exogenous NAD⁺ lowered the ER biomass (Fig. 5g,h) and reduced the ER stress signature (Fig. 5i).

Collectively, these data delineate a mechanistic connection between insufficient mitochondrial aspartate production, failed regeneration of the electron acceptor NAD⁺ and expansion of the ER membrane system.

GRP78/BiP is a master regulator for the ER stress response^{27,28}, capable of binding to all three major ER stress mediators (PERK, ATF6 and IRE1 α). Under ER stress conditions, BiP senses and binds to unfolded proteins, releasing PERK, ATF6 and IRE1, and triggering their respective ER stress pathways (Fig. 5j). Given the low NAD⁺ availability in RA T cells, we tested whether NAD⁺-dependent ADP ribosylation is relevant for BiP function. When compared with healthy T cells, a much lower fraction of BiP molecules in RA T cells was ADP ribosylated (Fig. 5k). The BiP-ADP-R^{lo} phenotype could be reproduced by blocking the electron transport chain with rotenone (Fig. 3l)

or piericidin A (Extended Data Fig. 7). By contrast, surplus exogenous NAD⁺ restored ADP ribosylation of BiP in RA T cells (Fig. 5m).

To link ADP ribosylation to BiP function, we analyzed the binding between BiP and its target protein IRE1 α by immunoprecipitation. Increasing doses of rotenone disrupted the binding of BiP to IRE1 α (Fig. 5n), whereas NAD⁺ supplementation doubled BiP–IRE1 α complex formation (Fig. 5o).

Together, these data define NAD⁺-dependent ADP ribosylation of BiP as an on–off switch of ER stress signals, placing mitochondrial fitness upstream of ER size and function, and specifying aspartate as a mitochondria-to-ER messenger.

Expansion of rough ER increases co-translational translocation.

To explore the functional consequence of ER expansion in RA T cells, we focused on cytokine production/secretion, which relies heavily on the endomembrane system. We first quantified ribosome-rich rough ER in healthy and patient-derived T cells (Fig. 6a–d). ER biomass was expanded in RA T cells, as indicated by the increased load of the ER chaperone calnexin, whereas global ribosomal protein levels were indistinguishable in healthy and RA T cells (Fig. 6a,b). To relate the expansion of the ER in RA T cells to their functional behavior, we focused on the ribosome-bonded rough ER, responsible for co-translational translocation. Immunoblotting showed high purity of rough ER when isolated out of the T cell cytosol (Extended Data Fig. 8a). T cells responded to activation with a dramatic increase in the ribosome-occupied rough ER membrane system (Extended Data Fig. 8b). RA T cells had a greater than twofold enlargement of ribosome-occupied ER membrane sheets (Fig. 6c,d).

Membrane-integrated and secretory protein synthesis involves localization of ribosomes to the cytosolic surface of the ER and co-translational docking of the mRNA–ribosome complex on the

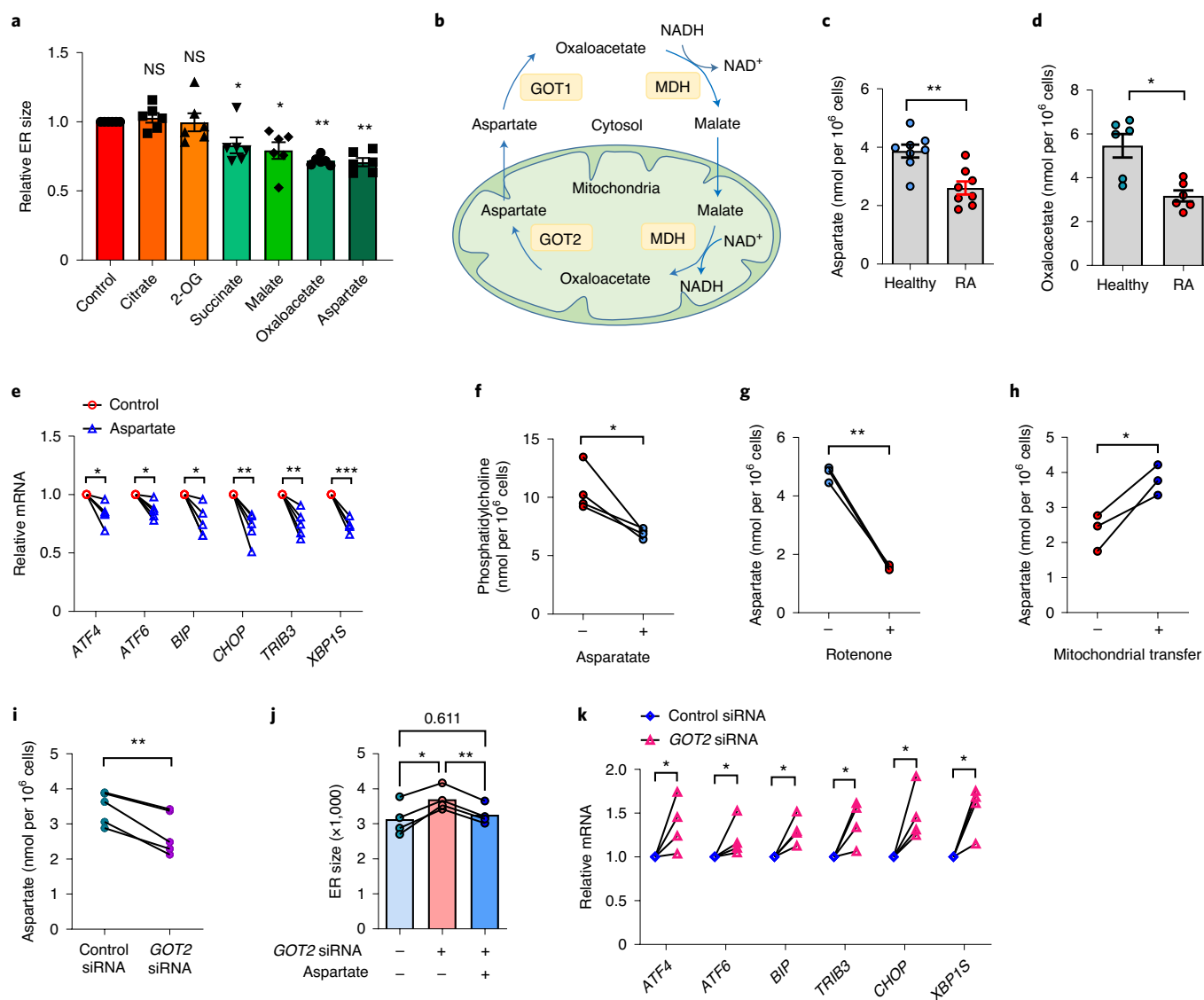


Fig. 3 | Mitochondria-derived aspartate controls ER size. Naive CD4⁺CD45RA⁺ T cells from patients with RA and age-matched healthy individuals were stimulated for 72 h. **a**, Mitochondrial intermediates determine ER size. RA T cells were supplemented with the indicated mitochondrial intermediates (all 1 mM) and ER size was quantified flow cytometrically ($n=6$). NS, not significant. **b**, Scheme for the malate-aspartate shuttle. MDH, malate dehydrogenase. **c,d**, RA T cells that are aspartate/oxaloacetate deficient: intracellular aspartate (healthy: $n=8$; RA: $n=8$) (**c**) and oxaloacetate (healthy: $n=6$; RA: $n=6$) (**d**) concentrations in T cells. **e,f**, Aspartate inhibits ER stress signals and phosphatidylcholine synthesis. RA T cells were treated with aspartate for 3 d. ER stress gene expression ($n=5$) (**e**) and phosphatidylcholine content ($n=4$) (**f**) were measured. **g,h**, Aspartate concentrations are dependent on intact mitochondrial function. Intracellular aspartate concentrations were measured after treatment of healthy T cells with the complex I inhibitor rotenone (**g**; 10 nM; $n=3$) or after the transfer of healthy mitochondria into RA T cells (**h**; $n=3$). **i-k**, GOT2 regulates ER size. GOT2 was knocked down by siRNA in healthy T cells. **i**, Intracellular aspartate levels ($n=5$). **j**, ER size quantified by flow cytometric analysis (ER Tracker MFI) ($n=4$). **k**, ER stress genes quantified by qPCR ($n=4$). All data are mean \pm s.e.m. One-way ANOVA and post-ANOVA, pair-wise, two-group comparisons conducted with Tukey's method (**a,j**). P values from comparison with control group: two-tailed paired Student's t -test (**e-i, k**); two-tailed, unpaired Mann-Whitney-Wilcoxon rank test (**c,d**): * $P < 0.05$, ** $P < 0.01$, *** $P < 0.001$.

ER membrane^{29,30}. To understand the functional implications of the enlarged rough ER in RA T cells, we analyzed mRNAs contained in the ER-bonded ribosomes. Considering that the rough ER sheets serve as the main site of synthesis for secreted and membrane-integrated proteins, we concentrated on T cell effector cytokines. In naive CD4⁺ T cells, transcripts for the lineage-determining effector cytokines IFN- γ , IL-4 and IL-17 were barely detectable, but IL2 and, even more so, TNF mRNA were abundant (Fig. 6e). Considering the critical role of TNF in the RA disease process, we focused on the transcription and translation of this cytokine. The overall pool of

TNF mRNA in resting and stimulated T cells from healthy individuals and patients was indistinguishable (Fig. 6f). To explore whether the expansion of ER membrane sheets in RA T cells impacts TNF transcription, ER-bound mRNAs were measured after phorbol 12-myristate 13-acetate/ionomycin (PMA/ION) activation. As expected, nonsecretory cytoplasmic proteins, including the glycolytic enzyme glyceraldehyde-3-phosphate dehydrogenase and the cytoskeletal protein actin, were underrepresented among ER-bound mRNAs (Fig. 6g). The mRNAs for the four cytokines, IFN- γ , IL-2, IL-17 and TNF, were all highly enriched, with IL2 and TNF mRNA

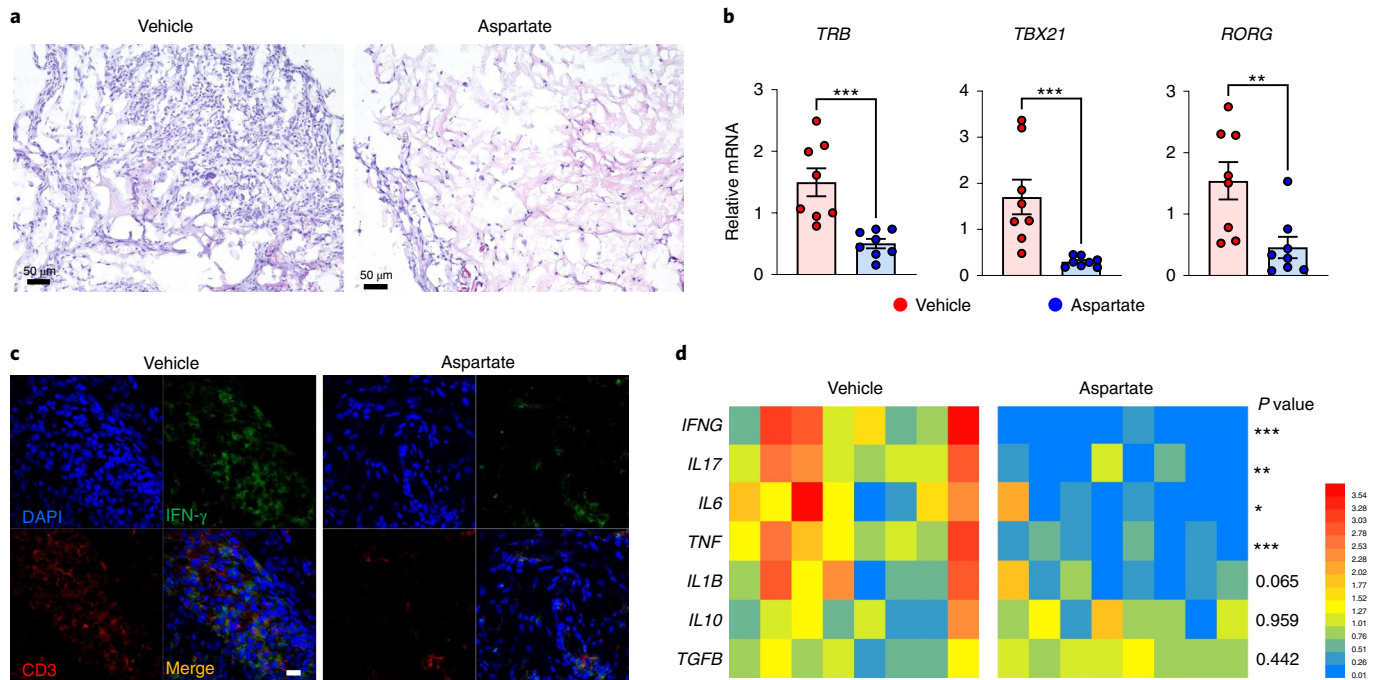


Fig. 4 | Aspartate is anti-inflammatory. Synovitis was induced in chimeric mice engrafted with human synovial tissue and immunoreconstituted with RA PBMCs. Chimeras were treated intraperitoneally with vehicle or aspartate (5 mg kg^{-1}). **a**, Representative hematoxylin and eosin (H&E) staining of explanted synovial tissue ($n=8$). **b**, Tissue transcriptomic analysis (qPCR) of synovial explants. Shown are data for *TRB* transcripts and the lineage-determining transcription factors *TBX21* and *RORC* ($n=8$). **c**, Representative image of coimmunofluorescence staining for IFN- γ -producing CD3⁺ T cells in the synovial tissue ($n=8$). Scale bar, 10 μm . **d**, Tissue transcriptomic analysis of major inflammatory cytokines (eight tissues in each study arm). All data are mean \pm s.e.m. Two-tailed, unpaired Mann-Whitney-Wilcoxon rank test: * $P < 0.05$, ** $P < 0.01$, *** $P < 0.001$.

being >100-fold more abundant at the ER membrane (Fig. 6g). With their expanded ER morphology, RA CD4⁺ T cells recruited a higher proportion of *TNF* mRNA to the organelle's surface (Fig. 6h), where selected mRNAs become subject to co-translational translocation³¹.

T cells rich in rough ER are TNF superproducers. The redistribution of *TNF* mRNA resulted in highly efficient TNF biogenesis (Fig. 7a–c). In patient-derived T cells, confocal imaging revealed a strong signal for TNF colocalizing with calnexin as well as being embedded into the plasma membrane (Fig. 7a). Intracellular staining yielded higher concentrations of TNF protein in RA compared with healthy T cells (Fig. 7b). Quantification of secreted TNF confirmed the increased cytokine release in patient-derived cells (Fig. 7c). We tested whether the unfolded protein response, a stress response program triggered by the accumulation of unfolded proteins in the ER lumen, is sufficient to enhance TNF biogenesis and can mimic the ER^{rich} phenotype of RA T cells. Treatment of healthy CD4⁺ T cells with tunicamycin failed to upregulate TNF synthesis (Extended Data Fig. 9a,b), suggesting that the mitochondria-induced ER expansion in RA T cells represents a state of ER stress without ER dysfunction.

The mechanistic link between ER expansion and enhanced recruitment of *TNF* mRNA to the ER surface, resulting in a TNF superproducer phenotype, raised the question of whether correcting the growth of the endomembrane system could repair uncontrolled cytokine release, disrupting mitochondrial function with the respiration inhibitors rotenone and piericidin A or knocking down *GOT2* mRNA transformed healthy T cells into TNF^{hi} producers (Fig. 7d–f). *GOT2* loss of function could be rescued by supplementation of aspartate (Fig. 7f). Two interventions repaired the excessive TNF secretion of RA T cells: the supplementation of exogenous aspartate or NAD⁺ and the transfer of intact mitochondria into the patients' T cells (Fig. 7g–i). It is interesting that asparagine, the amino acid structurally similar to aspartate, failed to affect ER size

and TNF production (Extended Data Fig. 9c,d), indicating a unique role of aspartate in NAD⁺/NADH metabolism. Finally, we tested the metabolic intermediates pyruvate and α -ketobutyrate, which can regenerate NAD⁺ through a distinct mechanism³². Both metabolites inhibited ER expansion in RA T cells and suppressed TNF production (Extended Data Fig. 9e,f).

Collectively, these data indicate that the enlargement of ribosome-occupied ER sheets in RA T cells has profound implications for TNF biogenesis by enhancing the process of co-translational translocation (Fig. 7j).

High TNF production by CD4⁺ T cells is arthrogenic. TNF is a prime therapeutic target in RA and specific blockade of the cytokine is now considered standard therapy³³. The propensity of the patients' CD4⁺ T cells to release high amounts of TNF therefore raised the question of whether such T cells have disease relevance. Rheumatoid synovial lesions consist of a mixture of cell types, most prominently T cells, B cells, macrophages and synovial fibroblasts. To implicate some or all cell populations in TNF production, we first analyzed recently published single-cell RNA-sequencing data⁴. Tissue-residing T cells contained abundant amounts of *TNF* mRNA, whereas macrophages and B cells were low positive, and fibroblasts were negative. In a second step, we allocated TNF production to the different cellular subsets by determining intracellular TNF by flow cytometry. Synovial tissues from patients with RA were disaggregated and stimulated with lipopolysaccharide (LPS)/PMA/ION in the presence of the Golgi blocker Brefeldin A (BFA). Intracellular TNF was measured cytometrically in T cells (CD45⁺CD3⁺), B cells (CD45⁺CD19⁺) and macrophages (CD45⁺CD68⁺). In leukocyte-rich synovial tissues (Fig. 8a), 80% of T cells and B cells were TNF⁺, whereas only 40% of macrophages produced TNF (Fig. 8b,c). On a per-cell basis, TNF was highly abundant in T cells (Fig. 8d), multi-fold higher than in B cells and macrophages. In leukocyte-poor RA

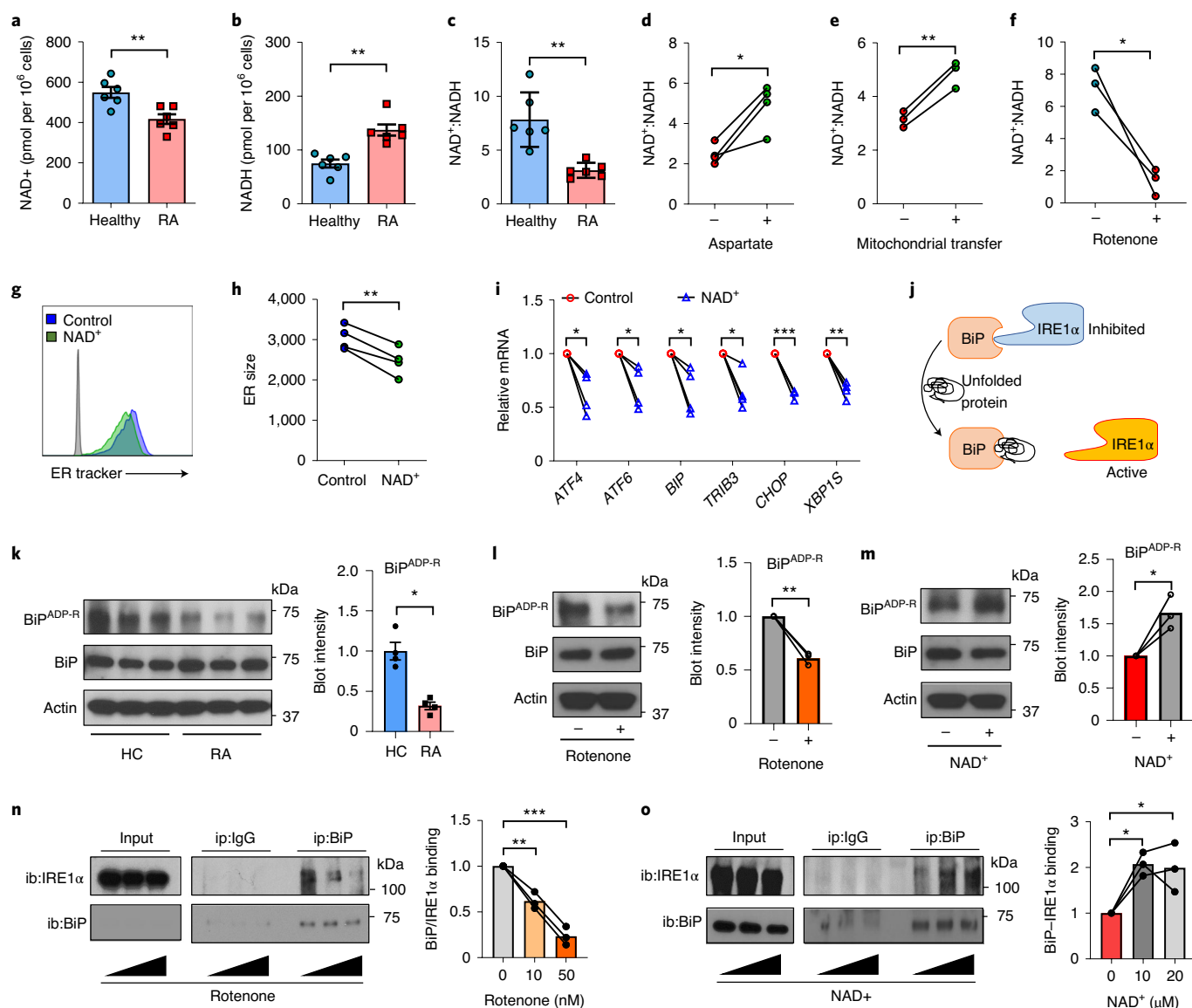


Fig. 5 | Aspartate is required for NAD⁺ regeneration and ADP ribosylation of BiP. Naive CD4⁺CD45RA⁺ T cells from patients with RA and age-matched healthy individuals were stimulated for 72 h. **a–c**, NAD⁺ deficiency in RA T cells. Quantification of intracellular NAD⁺ (**a**), NADH (**b**) and the NAD⁺:NADH ratio (**c**) in healthy and RA T cells ($n=6$). **d–f**, Aspartate and intact mitochondria regenerate NAD⁺. **d**, NAD⁺:NADH ratios in RA T cells treated with or without aspartate ($n=4$). **e**, NAD⁺:NADH ratios in RA T cells with or without mitochondrial transfer ($n=3$). **f**, NAD⁺:NADH ratios in healthy T cells treated with or without the complex I inhibitor rotenone (10 nM) ($n=3$). **g–h**, NAD⁺ controls ER size and ER stress. RA T cells were treated with or without NAD⁺. ER size was determined flow cytometrically (ER Tracker MFI). **g**, **h**, Representative histograms (**g**). ER size measurements from four experiments (**h**). **i**, ER stress gene expression profiling (qPCR) in RA T cells treated with or without NAD⁺ ($n=4$). **j–o**, NAD⁺-dependent ribosylation of BiP prevents ER expansion and stabilizes IRE1α binding. **j**, Scheme of IRE1α activity controlled by BiP in the ER lumen. **k**, ADP ribosylation of BiP in healthy (HC) and RA T cells ($n=3$). **l**, ADP ribosylation of BiP in healthy CD4⁺ T cells treated with or without rotenone (10 nM) for 24 h ($n=3$). **m**, ADP ribosylation of BiP in RA CD4⁺ T cells treated with or without NAD⁺ (10 μM) for 24 h ($n=3$). **n**, BiP-IRE1α binding in healthy CD4⁺ T cells treated with 0, 10 and 50 nM rotenone for 24 h ($n=3$). **o**, BiP-IRE1α binding in activated RA CD4⁺ T cells treated with 0, 10 and 20 μM NAD⁺ for 24 h ($n=3$). All data are mean \pm s.e.m. Two-tailed, unpaired Mann-Whitney-Wilcoxon rank test (**a–c**, **k**); two-tailed, paired Student's *t*-test (**d–i**); one-way ANOVA and post-ANOVA, pair-wise, two-group comparisons conducted with Tukey's method (**n**, **o**): ** $P < 0.05$, *** $P < 0.01$, **** $P < 0.001$.

tissues, B cells were barely detected (Fig. 8e), but most T cells were able to produce high amounts of TNF (Fig. 8f–h).

To validate that TNF production is a feature of tissue-embedded cells and not just detectable after LPS/PMA/ION stimulation of disaggregated cells, we established a method for analyzing cytokine production in freshly harvested synovial tissues from patients with RA. Cytokine secretion from the cells was blocked by treating intact tissue slices with BFA for 4 h. Subsequently, cells were isolated from the tissue and intracellular TNF was detected by flow cytometry

(Fig. 8i–k). In fresh synovial tissues, about 40% of synovial CD68⁺ macrophages produced TNF, with or without BFA treatment, indicating intracellular retention of TNF in tissue-residing macrophages. By contrast, tissue-residing T cells appeared to immediately release TNF into the tissue microenvironment. The frequencies of TNF⁺ T cells increased 10- to 20-fold on BFA-induced secretion blockade (Fig. 8k). These data identified synovial T cells as a dominant cellular source of TNF, in both leukocyte-poor and leukocyte-rich tissue lesions.

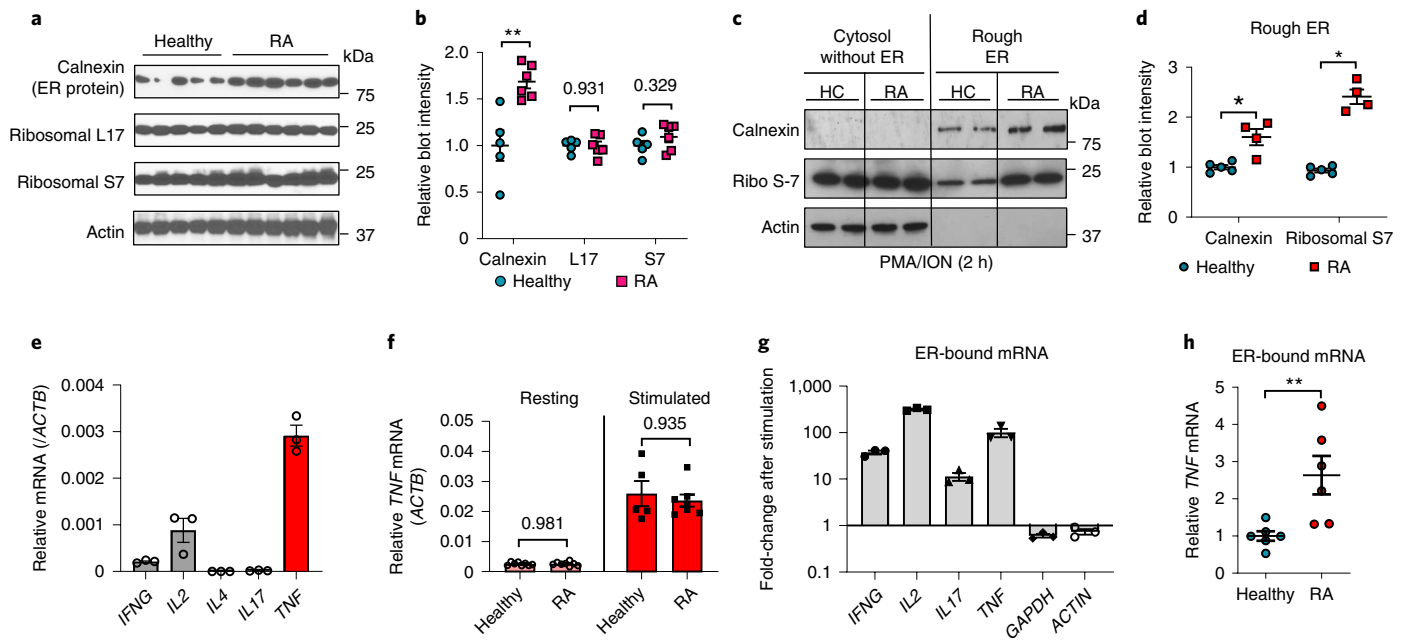


Fig. 6 | Expansion of the rough ER increases co-translational translocation in RA T cells. Naive CD4⁺CD45RA⁺ T cells from patients with RA and age-matched controls were stimulated for 72 h. **a–e**, Enrichment of rough ER in RA T cells. **a, b**, Immunoblot (**a**) and intensities (**b**) of the ER chaperon protein calnexin and the ribosomal proteins L17 and S7 in CD4⁺ T cells from five healthy individuals and six patients with RA. **c, d**, Rough ER isolated from healthy and RA T cells 2 h after restimulation. **c**, Calnexin, ribosomal S7 and β -actin quantified by immunoblotting. HC, healthy control. **d**, Quantification of blot intensity for rough ER in each group ($n=5$ healthy and 4 RA). **e**, TNF as the predominant cytokine expressed by activated naive CD4⁺ T cells. Transcripts for T cell effector cytokines in activated naive CD4⁺ T cells are quantified by qPCR ($n=3$). **f**, Healthy and RA T cells expressing a similar level of *TNF* mRNA. *TNF* mRNA concentrations are shown in healthy and RA T cells before ($n=8$ healthy and 8 RA) and after ($n=5$ healthy and 7 RA) PMA/ION stimulation. **g**, T cell stimulation induces enrichment of ER-bound mRNA for secretory proteins. Fold-change of ER-bound mRNA for secretory proteins and intracellular proteins after PMA/ION stimulation ($n=3$) is shown. **h**, Enrichment for ER-bound *TNF* mRNA in RA T cells. Rough ER was isolated from healthy and RA T cells 2 h after stimulation; mRNA associated with rough ER was quantified by qPCR ($n=6$). All data are mean \pm s.e.m. Two-tailed, unpaired Mann–Whitney–Wilcoxon rank test (**b, d, f, h**): * $P < 0.05$, ** $P < 0.01$.

To investigate whether T cell-derived TNF is relevant for synovial inflammation, we relied on a humanized mouse model in which human synovial tissue is engrafted into NSG mice and the chimeric host is immunoreconstituted with PBMCs from patients with RA^{19,34}. Before the PBMC transfer, FACS-sorted CD4⁺ T cells were transfected with control small interfering (si)RNA or siRNA-targeting *TNF*. The knockdown lowered *TNF* transcripts to about 50% of controls, mimicking a physiological situation. Histological evaluation of explanted synovial tissues demonstrated that suppressing T cell-derived TNF was strongly anti-inflammatory. Control chimeras, injected with control siRNA-transfected CD4⁺ T cells, developed robust synovitis. Tissues harvested from the control mice were densely infiltrated with CD3⁺ T cells (Fig. 8l,m). Tissue transcriptomic analysis revealed abundance of *TCR*, *TBX21* and *RORC* transcripts (Fig. 8n). CD4⁺ T cells with intact TNF production infiltrated into the synovial tissue space and triggered induction of *IFNG*, *IL17*, *IL21*, *TNF*, *IL6* and *IL1B* transcription (Fig. 8n). Synovial explants harvested from mice reconstituted with CD4⁺TNF^{lo} T cells had few tissue-infiltrating cells (Fig. 8i), density of tissue-residing CD3⁺ T cells was low (Fig. 8m) and all inflammatory genes were expressed at low abundance (Fig. 8n). In a parallel approach, we tested whether reconstitution of intact mitochondria affected synovitis. Analysis of the synovial explants documented anti-inflammatory potency of mitochondrial transfer. Synovial grafts harvested from mice reconstituted with RA T cells transferred with intact mitochondria had few tissue-infiltrating cells (Extended Data Fig. 10a) and low-density CD3⁺ T cell infiltrates (Extended Data Fig. 10b). Transcripts for major inflammatory genes were consistently low (Extended Data Fig. 10c). Collectively, these data

established that TNF-producing T cells preferentially home to the synovial tissue environment, and are indispensable for the induction and maintenance of synovitis.

Discussion

Recognition of autoantigen has been considered the major mechanism of autoimmunity, but recent studies have emphasized the importance of the intracellular environment in regulating T cell tolerance. Specifically, metabolic conditions have emerged as a guide to pathogenic T cell functions, with a failure of mitochondrial function and misdirected protein trafficking promoting differentiation of RA CD4⁺ T cells into short-lived effector cells, prone to execute tissue damage^{15,18,21}. A critical effector pathway in RA is the unrestrained production of TNF, a defect exploited by anti-TNF therapeutics. Data presented in the present study attribute TNF release to tissue-residing T cells that have dysfunctional mitochondria, a bloated, ribosome-bonded ER and highly efficient co-translational translocation. The molecular components of this pathogenic pathway begin with inadequate mitochondrial aspartate synthesis causing deficient regeneration of cytoplasmic NAD⁺, and sensing this defect by the ER through failed ADP ribosylation of the ER chaperone BiP. Unribosylated BiP releases IRE1 α , prompting expansion of ribosome-occupied ER sheets. Implicating the protein synthesis function of the ER in RA pathogenesis adds a new dimension to the conceptual understanding of autoimmunity and provides new strategies to treat tissue inflammation by replenishing aspartate, restoring BiP ADP ribosylation or interfering with co-translational translocation.

Although organelle function is recognized as a critical determinant of T cell antigen responsiveness, a role for ER morphology in

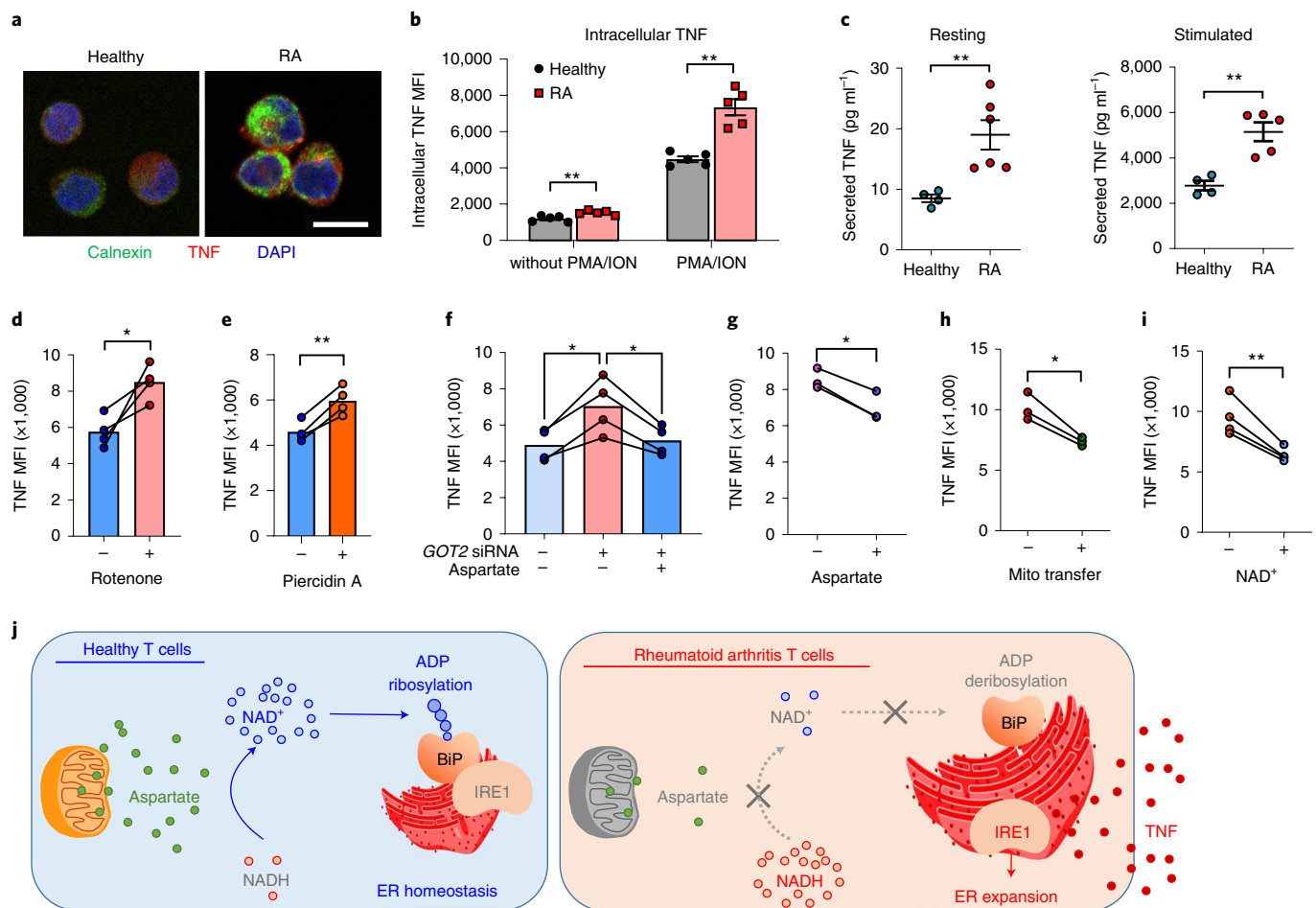
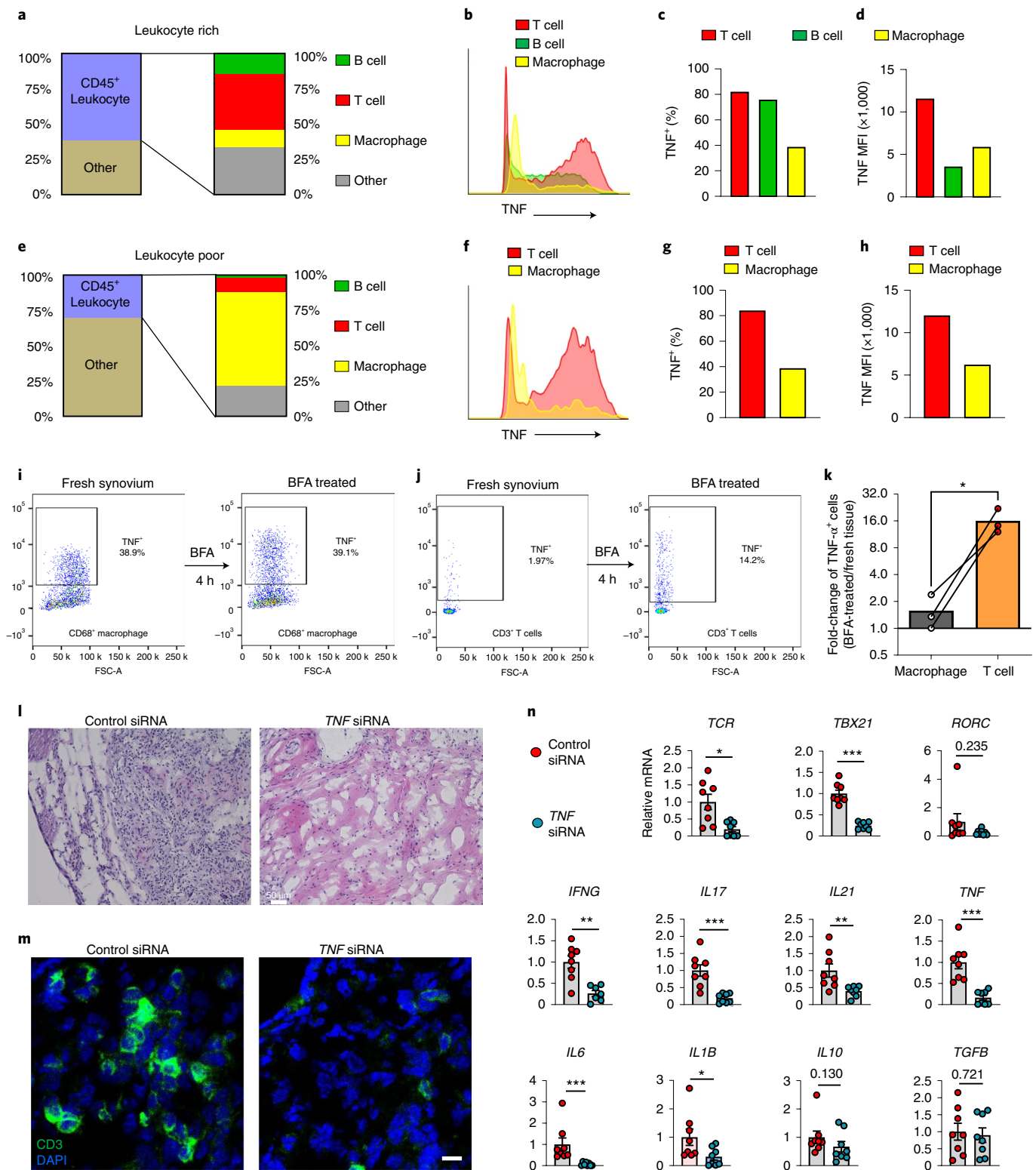


Fig. 7 | ER^{rich} RA T cells are TNF superproducers. Naïve CD4⁺CD45RA⁺ T cells from patients with RA and age-matched controls were stimulated for 72 h. **a**, Representative confocal image of the ER chaperone protein calnexin and TNF in healthy and RA T cells ($n=3$ independent experiments). Scale bar, 10 μ m. **b**, Flow cytometric measurement of intracellular TNF in CD4⁺ T cells from patients with RA and healthy individuals before and after PMA/ION stimulation (healthy: $n=5$; RA: $n=5$). **c**, TNF secreted into the extracellular space by unstimulated (healthy: $n=4$; RA: $n=6$) and stimulated (healthy: $n=4$; RA: $n=5$) RA and control CD4⁺ T cells. **d–i**, Mitochondrial function and aspartate controlling TNF production. **d,e**, Electron transfer inhibited in healthy T cells with rotenone (10 nM) or piericidin A (10 pM). TNF was measured by flow cytometry ($n=4$ in each series). **f**, GOT2 knockdown in healthy T cells, combined with or without aspartate rescue. TNF was measured by flow cytometry ($n=4$). **g**, TNF production in RA T cells treated with or without aspartate ($n=3$). **h**, TNF production in RA T cells reconstituted with or without healthy mitochondria ($n=3$). **i**, TNF production in RA T cells treated with or without NAD⁺ ($n=4$). **j**, Scheme showing the aspartate–NAD⁺–BiP pathway controlling TNF secretion. All data are mean \pm s.e.m. Two-tailed, unpaired Mann–Whitney–Wilcoxon rank test (**b,c**); two-tailed paired Student's *t*-test (**d–i**): * $P < 0.05$, ** $P < 0.01$, *** $P < 0.001$.

autoimmunity has not been proposed. Current data implicate ER size, function and co-translational translocation in TNF biogenesis, and thus in proinflammatory T cell effector functions. As the major site of protein synthesis, folding and transport, ER function ultimately governs the fate of secretory cytokines. Functional analysis of T cells mapped the underlying defect in unconstrained TNF secretion to the expansion of ER membranes that provide surface docking sites for the recruitment of mRNA–ribosome complexes. The ER is considered to be a highly dynamic organelle, its structure rapidly adapting to the cellular environment. Consisting of sheets and tubules, the peripheral ER is believed to shift the ratio of these structures to best serve the cell's needs. Cells synthesizing large amounts of proteins favor formation of sheets, whereas cells involved in lipogenesis preferentially build tubules³². Although the ER's role in handling cellular stress is well established, signals determining ER size and shape are less well defined. The transcription factor XBP-1 appears to be essential in ER biogenesis, possibly by controlling secretory pathway genes and membrane phospholipid synthesis^{23,35}. Data presented in the present study predict that it is

the morphology of the ER that deviates protective immunity to tissue-damaging immunity and exposes the host to uncontrolled TNF release.

Mechanistic experiments localized the signal upstream of the ER defect to the mitochondria. As the hub for protein, lipid and steroid synthesis, the ER most closely communicates with mitochondria to assess bioenergetic state and needs. ER–mitochondria communicate through membrane contacts³⁶, but could also involve soluble messengers. Disruption of ER–mitochondria interactions triggers ER stress responses^{37–39}, whereas ER-stressed cells tend to increase mitochondrial activity and ATP production to restore energy reservoirs^{40,41}. However, prolonged ER stress induces mitochondrial swelling and functional collapse and, if unresolved, results in mitochondria-dependent cell death. Information flux from the ER to the mitochondria relies largely on calcium transduced from ER stores to the mitochondrial matrix. The opposite direction of information flux, mitochondria affecting ER homeostasis, has remained elusive. As direct signaling between the ER and the mitochondria is mostly facilitated by tubular structures, we suspected



secreted mitochondrial intermediates of driving the expansion of ER sheets. Screening mitochondrial metabolites implicated succinate and its oxidation products in communicating the metabolic state of mitochondria, whereas 2-OG was ineffective in inducing ER shape changes. Oxaloacetate and its downstream product, the amino acid aspartate, were most effective in controlling ER expansion. Aspartate functions as a critical component of the malate-aspartate shuttle, responsible for transporting electrons across the mitochondrial membrane through conversion of NADH to NAD⁺.

Pinpointing aspartate as the mitochondrial messenger governing ER morphology placed the sensing mechanism in the cytoplasm.

ER^{rich} RA T cells were poor in aspartate, had accumulated NADH and lacked the hydrogen/electron acceptor NAD⁺. The shortage of aspartate resulted from a combination of two mitochondrial defects: one in the TCA cycle providing insufficient carbon backbone and one in the electron transport chain failing to deliver NAD⁺. We have defined two molecular defects in the mitochondria of RA T cells^{18,20}. Faulty repair of mitochondrial DNA results in a nonfunctional

Fig. 8 | TNF-producing CD4⁺ T cells function as arthritogenic effector cells. a,e. Cellular composition of leukocyte-rich and leukocyte-poor tissues collected from patients with rheumatoid synovitis. **b-d,f-h.** TNF as a product of tissue T cells. Flow cytometric analysis of intracellular TNF in T cells, B cells and macrophages after stimulation with LPS/PMA/ION/BFA for 4 h is shown. Histogram of TNF staining (**b,f**). Frequencies of TNF-producing cell populations (**c,g**). MFI of TNF staining in different cell populations (**d,h**). **i-k.** Spontaneous TNF production in T cells and macrophages residing in the synovium. Freshly harvested synovial tissue from patients with RA was incubated with or without the secretion inhibitor BFA for 4 h, before cells were dissociated from the tissue and intracellular TNF was detected by flow cytometry. TNF⁺CD45⁺CD68⁺ macrophages (**i**) and TNF⁺CD45⁺CD3⁺ T cells (**j**) are shown in synovial tissue before and after BFA treatment. Fold-change in the frequency of TNF⁺ macrophage and TNF⁺ T cells after BFA treatment (**k**, $n = 3$ tissues). **l-n.** TNF-producing CD4⁺ T cells, an absolute requirement for rheumatoid synovitis. Rheumatoid synovitis was induced in human synovial tissues engrafted into NSG mice. CD4⁺ T cells from patients with RA were transfected with control or *TNF* siRNA and adoptively transferred into the chimeric mice. Synovial grafts were explanted 2 weeks later. H&E staining of explanted synovial tissues. Scale bar, 50 μm (**l**). Immunofluorescence staining of CD3⁺ T cells in synovial infiltrates. Scale bar, 10 μm (**m**). Synovial tissue transcriptome for *TRB*, *TBET*, *RORG* and other inflammatory markers as indicated (**n**, $n = 8$). All data are mean \pm s.e.m. Two-tailed, paired Student's *t*-test (**k**); two-tailed, unpaired Mann-Whitney-Wilcoxon rank test (**n**): * $P < 0.05$, ** $P < 0.01$, *** $P < 0.001$.

respiration chain²⁰ and transcriptional repression of the succinate-CoA ligase guanosine diphosphate-forming subunit β (SUCLG2) leads to reversal of the TCA by intersecting the production of succinate¹⁸. Thus, the aspartate¹⁰ state of RA T cells is a consequence of mitochondrial malfunction.

Supporting aspartate biosynthesis is an essential role of mitochondrial respiration^{32,42}, designating the amino acid as an ideal messenger of mitochondrial intactness. Aspartate exits mitochondria to function as an electron acceptor in the cytosol, facilitating the regeneration of NAD⁺ from NADH. The mitochondrial inner membrane is impermeable to oxaloacetate⁴³, relying on aspartate to shuttle electrons across the membrane. Replenishing aspartate was highly effective in re-educating RA T cells. Aspartate supplementation was sufficient to reverse the inflated ER membrane system and had potent anti-inflammatory effects in vivo, validating the relevance of mitochondria-ER communication in autoimmune tissue inflammation.

Ultimately, aspartate deficiency reflected the failure of the electron transport chain and at the same time aggravated cytoplasmic NAD⁺ shortage. The ER senses NAD⁺ deficiency by relying on NAD's function as a cosubstrate for post-translational modification, specifically the ADP ribosylation of an ER-positioned protein. The ER chaperone and signaling regulator GRP78/BiP monitors ER stress signals by controlling the activation of the transmembrane ER stress sensors (IRE1, PERK and ATF6) through a binding-release mechanism^{44,45}. On sensing and binding of unfolded proteins, BiP releases IRE1, PERK and ATF6, activating parallel pathways in the ER stress program. The substrate-binding ability of BiP is fine-tuned by NAD⁺-dependent ADP ribosylation. The increasing burden of unfolded proteins in the ER results in decreased BiP ribosylation⁴⁶, whereas lowering of the unfolded protein flux stabilizes BiP-client binding through enhanced ADP ribosylation. Two potential ADP-ribosylation sites (Arg470, Arg492) have been identified within BiP's substrate-binding domain, with ADP ribosylation destabilizing the binding of peptide substrates and inactivating the chaperone. Data presented in the present study directly linked intracellular NAD⁺ concentrations to BiP ribosylation. In aspartate¹⁰/NAD¹⁰ RA T cells, BiP was deribosylated and released the ER stress sensor IRE1, communicating mitochondrial malfunction to the ER membrane system. Both exogenous aspartate and NAD⁺ re-established ER homeostasis and corrected the proinflammatory phenotype of RA T cells. Conversely, targeting mitochondrial respiration in healthy T cells was sufficient to deplete intracellular aspartate and NAD⁺ generation, phenocopied the RA-associated ER expansion and induced TNF-superproducing effector cells. Also, knockdown of the aminotransferase GOT2 transformed healthy T cells into TNF-releasing proinflammatory effector cells, clearly identifying aspartate generation as the pinnacle defect.

Understood as a crucial pathogenic element in RA, T cells have adopted fundamentally different bioenergetic pathways that

directly underpin their disease-inducing properties. Characteristic traits, such as clonal expansion, cytokine release, migratory behavior and tissue invasiveness, are all dependent on alterations in fuel selection and handling of energy carriers¹⁹⁻²¹. Although extracellular signals, such as nutrient availability, have not been excluded as determining factors in the metabolic reprogramming, cell-intrinsic abnormalities seem to be causative⁴⁷. Cellular organelles, including lysosomes, mitochondria and the endomembrane system, are now recognized to contribute to RA by deviating T cell differentiation toward SLECs^{20,21,47}. Current data suggest a hierarchical order, with mitochondrial malfunction giving rise to ER reshaping and stress responses. Consequently, approaches to re-engineer autoaggressive RA T cells into host-protective memory T cells should focus on repairing the mitochondria. In an effort to explore new therapeutic strategies, we validated several therapeutic interventions in an in vivo system of synovial inflammation. Mitochondria-ER miscommunication, and the resulting excessive TNF production, could be repaired by transferring healthy mitochondria into RA T cells. Technically less demanding was the provision of exogenous NAD⁺ and aspartate, which suppressed TNF production and successfully restrained synovial tissue inflammation. Other metabolites capable of regenerating cytoplasmic NAD⁺ may be equally suitable for treating RA.

Direct targeting of TNF with biologic therapies has revolutionized the management of multiple autoimmune diseases^{33,48}. However, low rates of disease remission, the development of adverse effects and the generation of antibodies against biologic TNF inhibitors³³ all curb the efficacy of anti-TNF therapy. Defining TNF-superproducing T cells as the major perpetrator in synovial inflammation and rectifying the defect by replenishing missing mitochondrial metabolites may give rise to new classes of immunomodulatory therapies that interfere with upstream pathologies instead of inhibiting the final product of proinflammatory effector cells. Targeting the mitochondria-ER crosstalk may facilitate highly effective, pathogenesis-inspired therapeutic interventions.

Online content

Any methods, additional references, Nature Research reporting summaries, source data, extended data, supplementary information, acknowledgements, peer review information; details of author contributions and competing interests; and statements of data and code availability are available at <https://doi.org/10.1038/s41590-021-01065-2>.

Received: 1 April 2021; Accepted: 1 October 2021;
Published online: 22 November 2021

References

1. Deane, K. D., Norris, J. M. & Holers, V. M. Preclinical rheumatoid arthritis: identification, evaluation, and future directions for investigation. *Rheum. Dis. Clin. North Am.* **36**, 213-241 (2010).

2. Feldmann, M., Brennan, F. M. & Maini, R. N. Role of cytokines in rheumatoid arthritis. *Annu. Rev. Immunol.* **14**, 397–440 (1996).
3. Maini, R. N. & Taylor, P. C. Anti-cytokine therapy for rheumatoid arthritis. *Annu. Rev. Med.* **51**, 207–229 (2000).
4. Zhang, F. et al. Defining inflammatory cell states in rheumatoid arthritis joint synovial tissues by integrating single-cell transcriptomics and mass cytometry. *Nat. Immunol.* **20**, 928–942 (2019).
5. Rubbert-Roth, A. et al. Failure of anti-TNF treatment in patients with rheumatoid arthritis: the pros and cons of the early use of alternative biological agents. *Autoimmun. Rev.* **18**, 102398 (2019).
6. Grivnenkov, S. I. et al. Distinct and nonredundant *in vivo* functions of TNF produced by T cells and macrophages/neutrophils: protective and deleterious effects. *Immunity* **22**, 93–104 (2005).
7. Bovensiepen, C. S. et al. TNF-producing Th1 cells are selectively expanded in liver infiltrates of patients with autoimmune hepatitis. *J. Immunol.* **203**, 3148–3156 (2019).
8. Jain, A. et al. T cells instruct myeloid cells to produce inflammasome-independent IL-1 β and cause autoimmunity. *Nat. Immunol.* **21**, 65–74 (2020).
9. Schreurs, R. et al. Human fetal TNF- α -cytokine-producing CD4⁺ effector memory T cells promote intestinal development and mediate inflammation early in life. *Immunity* **50**, 462–476.e468 (2019).
10. Weyand, C. M. & Goronzy, J. J. T-cell-targeted therapies in rheumatoid arthritis. *Nat. Clin. Pr. Rheumatol.* **2**, 201–210 (2006).
11. Weyand, C. M. & Goronzy, J. J. Immunometabolism in early and late stages of rheumatoid arthritis. *Nat. Rev. Rheumatol.* **13**, 291–301 (2017).
12. Slowikowski, K., Wei, K., Brenner, M. B. & Raychaudhuri, S. Functional genomics of stromal cells in chronic inflammatory diseases. *Curr. Opin. Rheumatol.* **30**, 65–71 (2018).
13. Isaacs, J. D. Therapeutic T-cell manipulation in rheumatoid arthritis: past, present and future. *Rheumatology* **47**, 1461–1468 (2008).
14. Probert, L. et al. Wasting, ischemia, and lymphoid abnormalities in mice expressing T cell-targeted human tumor necrosis factor transgenes. *J. Immunol.* **151**, 1894–1906 (1993).
15. Weyand, C. M. & Goronzy, J. J. The immunology of rheumatoid arthritis. *Nat. Immunol.* **22**, 10–18 (2021).
16. Yang, Z. et al. Restoring oxidant signaling suppresses proarthritogenic T cell effector functions in rheumatoid arthritis. *Sci. Transl. Med.* **8**, 331ra338 (2016).
17. Yang, Z., Fujii, H., Mohan, S. V., Goronzy, J. J. & Weyand, C. M. Phosphofructokinase deficiency impairs ATP generation, autophagy, and redox balance in rheumatoid arthritis T cells. *J. Exp. Med.* **210**, 2119–2134 (2013).
18. Wu, B. et al. Succinyl-CoA ligase deficiency in pro-inflammatory and tissue-invasive T cells. *Cell Metab.* **32**, 967–980.e965 (2020).
19. Shen, Y. et al. Metabolic control of the scaffold protein TKS5 in tissue-invasive, proinflammatory T cells. *Nat. Immunol.* **18**, 1025–1034 (2017).
20. Li, Y. et al. The DNA repair nuclease MRE11A functions as a mitochondrial protector and prevents T cell pyroptosis and tissue inflammation. *Cell Metab.* **30**, 477–492.e476 (2019).
21. Wen, Z. et al. N-Myristoyltransferase deficiency impairs activation of kinase AMPK and promotes synovial tissue inflammation. *Nat. Immunol.* **20**, 313–325 (2019).
22. Bommiasamy, H. et al. ATF6 α induces XBP1-independent expansion of the endoplasmic reticulum. *J. Cell Sci.* **122**, 1626–1636 (2009).
23. Sriburi, R., Jackowski, S., Mori, K. & Brewer, J. W. XBP1: a link between the unfolded protein response, lipid biosynthesis, and biogenesis of the endoplasmic reticulum. *J. Cell Biol.* **167**, 35–41 (2004).
24. Martinez-Reyes, I. & Chandel, N. S. Mitochondrial TCA cycle metabolites control physiology and disease. *Nat. Commun.* **11**, 102 (2020).
25. Zaslona, Z. & O'Neill, L. A. J. Cytokine-like roles for metabolites in immunity. *Mol. Cell* **78**, 814–823 (2020).
26. Chinopoulos, C. Acute sources of mitochondrial NAD⁺ during respiratory chain dysfunction. *Exp. Neurol.* **327**, 113218 (2020).
27. Korennykh, A. & Walter, P. Structural basis of the unfolded protein response. *Annu. Rev. Cell Dev. Biol.* **28**, 251–277 (2012).
28. Jager, R., Bertrand, M. J., Gorman, A. M., Vandenabeele, P. & Samali, A. The unfolded protein response at the crossroads of cellular life and death during endoplasmic reticulum stress. *Biol. Cell* **104**, 259–270 (2012).
29. Voorhees, R. M. & Hegde, R. S. Toward a structural understanding of co-translational protein translocation. *Curr. Opin. Cell Biol.* **41**, 91–99 (2016).
30. Elvekrog, M. M. & Walter, P. Dynamics of co-translational protein targeting. *Curr. Opin. Chem. Biol.* **29**, 79–86 (2015).
31. Schwarz, D. S. & Blower, M. D. The endoplasmic reticulum: structure, function and response to cellular signaling. *Cell. Mol. Life Sci.* **73**, 79–94 (2016).
32. Sullivan, L. B. et al. Supporting aspartate biosynthesis is an essential function of respiration in proliferating cells. *Cell* **162**, 552–563 (2015).
33. Rubbert-Roth, A. et al. TNF inhibitors in rheumatoid arthritis and spondyloarthritis: are they the same? *Autoimmun. Rev.* **17**, 24–28 (2018).
34. Li, Y. et al. Deficient activity of the nuclease MRE11A induces T cell aging and promotes arthritogenic effector functions in patients with rheumatoid arthritis. *Immunity* **45**, 903–916 (2016).
35. Shaffer, A. L. et al. XBP1, downstream of Blimp-1, expands the secretory apparatus and other organelles, and increases protein synthesis in plasma cell differentiation. *Immunity* **21**, 81–93 (2004).
36. Phillips, M. J. & Voeltz, G. K. Structure and function of ER membrane contact sites with other organelles. *Nat. Rev. Mol. Cell Biol.* **17**, 69–82 (2016).
37. Hayashi, T. & Su, T. P. Sigma-1 receptor chaperones at the ER-mitochondrion interface regulate Ca²⁺ signaling and cell survival. *Cell* **131**, 596–610 (2007).
38. Sebastian, D. et al. Mitofusin 2 (Mfn2) links mitochondrial and endoplasmic reticulum function with insulin signaling and is essential for normal glucose homeostasis. *Proc. Natl Acad. Sci. USA* **109**, 5523–5528 (2012).
39. Simmen, T. et al. PACS-2 controls endoplasmic reticulum-mitochondria communication and Bid-mediated apoptosis. *EMBO J.* **24**, 717–729 (2005).
40. Knupp, J., Arvan, P. & Chang, A. Increased mitochondrial respiration promotes survival from endoplasmic reticulum stress. *Cell Death Differ.* **26**, 487–501 (2019).
41. Bravo, R. et al. Increased ER-mitochondrial coupling promotes mitochondrial respiration and bioenergetics during early phases of ER stress. *J. Cell Sci.* **124**, 2143–2152 (2011).
42. Birsoy, K. et al. An essential role of the mitochondrial electron transport chain in cell proliferation is to enable aspartate synthesis. *Cell* **162**, 540–551 (2015).
43. Davila, A. et al. Nicotinamide adenine dinucleotide is transported into mammalian mitochondria. *eLife* <https://doi.org/10.7554/eLife.33246> (2018).
44. Bettigole, S. E. & Glimcher, L. H. Endoplasmic reticulum stress in immunity. *Annu. Rev. Immunol.* **33**, 107–138 (2015).
45. Gardner, B. M., Pincus, D., Gotthardt, K., Gallagher, C. M. & Walter, P. Endoplasmic reticulum stress sensing in the unfolded protein response. *Cold Spring Harb. Perspect. Biol.* **5**, a013169 (2013).
46. Chambers, J. E., Petrova, K., Tomba, G., Vendruscolo, M. & Ron, D. ADP ribosylation adapts an ER chaperone response to short-term fluctuations in unfolded protein load. *J. Cell Biol.* **198**, 371–385 (2012).
47. Wu, B., Goronzy, J. J. & Weyand, C. M. Metabolic fitness of T cells in autoimmune disease. *Immunometabolism* <https://doi.org/10.20900/immunometab20200017> (2020).
48. Kalliolias, G. D. & Ivashkiv, L. B. TNF biology, pathogenic mechanisms and emerging therapeutic strategies. *Nat. Rev. Rheumatol.* **12**, 49–62 (2016).

Publisher's note Springer Nature remains neutral with regard to jurisdictional claims in published maps and institutional affiliations.

© The Author(s), under exclusive licence to Springer Nature America, Inc. 2021

Methods

Patients and samples. Patients enrolled in the study fulfilled the diagnostic criteria for RA and tested positive for rheumatoid factor and/or anti-CCP antibodies. All patients ($n=120$) recruited had active disease. The clinical characteristics are presented in Supplementary Table 1. The following criteria excluded individuals from enrollment: current or previous diagnosis of cancer, uncontrolled medical disease and chronic inflammatory syndromes. Age-matched healthy donors without a personal history of cancer or autoimmune disease served as controls. All patients and controls provided informed consent and they did not receive compensation. All studies were approved by the Institutional Review Board (IRB) at Stanford and the IRB at the Mayo Clinic.

Cell preparation and culture. PBMCs were isolated by gradient centrifugation with Lymphocyte Separation Medium (Lonza). CD4⁺CD45RA⁺ naive T cells were isolated from PBMCs with the EasySep Human Naive CD4⁺ T Cell Enrichment Kit (Stemcell Technologies). Purity of cell populations was consistently >95%. Anti-CD3/anti-CD28-coated Dynabeads (Gibco) were used to activate naive CD4⁺ T cells at a ratio of 2 cells:1 bead for 72 h. Cell Activation Cocktail (PMA/ION) (BioLegend) was used to stimulate cytokine production in T cells with or without BFA (eBioscience) for 2 h.

Reagents. The pCMV5-Flag-XBP1s plasmid was purchased from Addgene. Human TNF siRNA, GOT2 siRNA and control siRNA were obtained from Thermo Fisher Scientific. The mitochondrial respiration inhibitors antimycin A, rotenone and oligomycin were purchased from Agilent Technologies, and piericidin A was from Cayman Chemical. NAD⁺ was obtained from Cayman Chemical. 2-OG, succinic acid, L-aspartic acid and L-asparagine were from Sigma-Aldrich. Malic acid was from Santa Cruz Biotechnology. MitoTrackerRed and MitoTrackerGreen were purchased from Thermo Fisher Scientific. Assay kits for aspartate, oxaloacetate, NAD⁺/NADH and phosphatidylcholine were obtained from Sigma-Aldrich. An ELISA kit for human TNF was from Thermo Fisher Scientific.

Intracellular TNF measurement. To measure intracellular TNF production, CD4⁺CD45RA⁺ naive T cells were activated for 72 h and stimulated with PMA/ION/BFA for 2 h. Paraformaldehyde, 4%, was used for fixation and 0.1% saponin to permeabilize the cells. Cells were stained with PE anti-human TNF antibody (1:100, BD, catalog no. 554513) for 1 h. Flow cytometry was performed on an LSR II flow cytometer (BD Biosciences). Data were analyzed with FlowJo software (Tree Star Inc).

Labeling of ER membranes. ER tracker green (Thermo Fisher Scientific, catalog no. E34251) was used to stain the ER-localized, ATP-sensitive K⁺ channels following the manufacturer's instructions. Flow cytometry was performed to detect ER tracker signal on an LSR II flow cytometer (BD Biosciences). The intensity of ER tracker staining was taken as a correlate of the size of the ER membranes. Data were analyzed with FlowJo software (Tree Star Inc).

Transmission electron microscopy. Cells were resuspended in McDowell's and Trump's fixative for 1 h at room temperature and then pelleted with a microcentrifuge. Cells were washed with 0.1 M phosphate buffer for 5 min (twice). Liquid agar was added to the cell pellet and the cells were resuspended, followed immediately by centrifugation. Once the sample had cooled, the agar was removed, and the sample pellet removed with a razor blade and placed into 0.1 M phosphate buffer. After 2 rinses in 0.1 M phosphate buffer, pH 7.2, the sample was placed in 1% osmium tetroxide in the same buffer for 1 h at room temperature. The sample was rinsed twice in distilled water and dehydrated in an ethanolic series, culminating in two changes of 100% acetone. The cell pellet was then placed in a mixture of Spurr resin and acetone (1:1) for 30 min, followed by 2 h in 100% resin with 2 changes. The cell pellet was placed into 100% Spurr resin in an embedding mold and polymerized at 65 °C for ≥12 h. Ultrathin (70–90 nm) sections were cut on an ultramicrotome with a diamond knife, stained with lead citrate and examined with a JEOL 1400 transmission electron microscope.

Rough ER isolation. Endoplasmic Reticulum Isolation Kit (Sigma-Aldrich, catalog no. ER0100) was used to isolate rough ER.

Measurement of MMP. MitoTrackerRed (Thermo Fisher Scientific, catalog no. M7512) is a fluorescent dye that stains mitochondria in live cells and its accumulation is dependent on MMP. Staining intensity was analyzed with an LSR II flow cytometer (BD Biosciences) and data were analyzed with FlowJo software (Tree Star Inc).

Immunoblotting. Cellular proteins or rough ER proteins were extracted with radioimmunoprecipitation buffer (Sigma-Aldrich). Protein expression levels were examined by immunoblotting as previously described⁴⁹. Monoclonal antibodies specific for ribosomal protein L17, ribosomal protein S7 and BiP were purchased from Santa Cruz Biotechnology. Antibodies specific for calnexin and IRE1 α were from Cell Signaling Technology. β -Actin expression detected with

anti- β -actin antibody (Cell Signaling Technology, catalog no. 8H10D10) served as the internal control.

Real-time PCR. Total RNA or rough ER-bound RNA was extracted with TRIzol (Thermo Fisher Scientific) and Direct-zol RNA MiniPrep Kit (ZYMO Research). Complementary DNA was synthesized using Maxima First Strand cDNA Synthesis Kits (Thermo Fisher Scientific). Quantitative (q)PCR analyses were performed using SYBR Green qPCR Master Mix (Bimake) and gene expression was normalized to *ACTB* transcripts. The primers are listed in Supplementary Table 2.

Mitochondrial transfer. On day 0, naive CD4⁺ T cells from a healthy donor were isolated and activated with anti-CD3/CD28 beads. On day 3, naive CD4⁺ T cells from patients with RA were purified and activated. On day 5, 4 million healthy CD4⁺ T cells were harvested, and mitochondria were isolated using Mitochondria Isolation Kit for Cultured Cells (Thermo Fisher Scientific, catalog no. 89874). In parallel, 0.2 million activated RA CD4⁺ T cells were collected and spun at 300g for 5 min. Resuspended cells were mixed with the mitochondrial suspension and carefully resuspended. The cell/mitochondria mixture and the control cell/phosphate-buffered saline mixture were centrifuged at 1,500g for 5 min. After washing, the cells were stimulated with anti-CD3/CD28 beads for 1 d more.

Human synovial tissue–NSG mouse chimeras. As previously reported⁵⁰, NSG mice from the Jackson Laboratory were maintained and bred under specific pathogen-free conditions on a 12:12 h light:dark cycle at 20–22 °C with free access to water and food. Animal housing facilities were monitored for infection with specific pathogens every 6 weeks and the health status of all animals was checked daily. Both male and female mice were randomly used at age 8–12 weeks. After 7 d, the mice were infused with 10 million PBMCs collected from patients with RA with active disease. In some experiments, CD4⁺ T cells in PBMCs were FACS sorted and transfected with siRNA-targeting TNF or control siRNA, before the cells were injected into the mice. Alternatively, healthy mitochondria were transferred into RA CD4⁺ T cells before the immune reconstitution. For these experiments, CD4⁺ T cells were FACS sorted and mitochondria from healthy T cells were transferred into RA CD4⁺ T cells as described above. On day 14, synovial tissues were explanted from the chimeric mice, embedded in optimal cutting temperature (OCT; Sakura Finetek, catalog no. 4583) or shock-frozen for further experiments (tissue staining or RNA extraction). All in vivo experiments were carried out in accordance with the guidelines of the Institutional Animal Care and Use Committee.

Immunohistochemistry. Frozen sections of synovial tissues were stained with mouse anti-human CD3 (1:100; DAKO, clone F7.2.38) and rabbit anti-human IFN- γ (1:100, Abcam, catalog no. 4583ab25101). Alexa Fluor-594 anti-mouse immunoglobulin G (IgG) (1:200, Thermo Fisher Scientific, catalog no. 4583A-11032) and Alexa Fluor-488 anti-rabbit IgG (1:200, Thermo Fisher Scientific, catalog no. 4583A-11034) were used as secondary antibodies. Images of CD3/IFN- γ staining were obtained using a LSM710 confocal microscope (Carl Zeiss) with a Plan-Neofluar $\times 40/1.3$ -numerical aperture (NA) oil objective lens.

Immunofluorescence. To visualize intracellular proteins, cells were collected, fixed with 4% paraformaldehyde for 10 min and permeabilized using 0.5% saporin. The following primary antibodies were used: anti-calnexin rabbit monoclonal antibody (1:100, Cell Signaling Technology) and anti-PDI mouse monoclonal antibody (1:100, Thermo Fisher Scientific). The following secondary antibodies were used: Alexa Fluor-594 goat anti-mouse IgG (1:200, Thermo Fisher Scientific, catalog no. A-11032) and Alexa Fluor-488 goat anti-rabbit IgG (1:200, Thermo Fisher Scientific, catalog no. A-11008). Nuclei were stained with DAPI. The LSM710 system (Carl Zeiss) with a Plan Apochromat $\times 63/1.40$ -NA oil DICIII objective lens (Carl Zeiss) was used to acquire images.

BiP ADP ribosylation. Activated naive CD4⁺ T cells, 5×10^6 , were lysed with immunoprecipitation (IP) lysis buffer (Thermo Fisher Scientific, catalog no. 87788) containing protease and phosphatase inhibitors. BiP protein in whole-cell lysates was pulled down by incubation with agarose-conjugated anti-BiP antibody (Santa Cruz Biotechnology, catalog no. sc-13539) for 4 h at 4 °C. Agarose was washed 5 \times with IP lysis buffer and boiled for 5 min in loading buffer. Eluted protein was separated by sodium dodecylsulfate (SDS)–polyacrylamide gel electrophoresis (PAGE) and ADP-ribosylated BiP was detected using antibody against ADP-ribose (Cell Signaling Technology, catalog no. 83732).

BiP/ IRE1 α binding. Cells were lysed with IP lysis buffer (Thermo Fisher Scientific, catalog no. 87788) containing protease and phosphatase inhibitors. Whole-cell lysates were incubated with 2 μ g of anti-BiP antibody (Santa Cruz Biotechnology, catalog no. sc-13539) and Protein A/G PLUS-Agarose (Santa Cruz Biotechnology, catalog no. sc-2003) for 4 h at 4 °C. Normal rat IgG (Santa Cruz Biotechnology, catalog no. sc-2026) was used as the IgG control. The immunocomplexes were washed with IP lysis buffer 5 \times , then eluted with loading buffer and separated by SDS–PAGE. Immunoblotting for IRE1 α was performed following standard procedures for immunoblotting.

Quantification and statistical analysis. Statistical analyses were performed using GraphPad Prism software. To compare data within two groups, the paired Wilcoxon's test or the Mann–Whitney test was used when the sample size per group was >5 . Parametric Student's *t*-test was used only if the sample size per group was ≤ 5 . To adjust for multiple testing, we used Hochberg's step-down method to control for a family-wise-error rate at the 0.05 levels. One-way analysis of variance (ANOVA) was used and pair-wise comparison using Tukey's method was applied for comparisons across ≥ 3 groups. All data points were included in the analysis and no outliers were detected using Grubbs' test. All data are presented as mean \pm s.e.m. * $P < 0.05$, ** $P < 0.01$, *** $P < 0.001$ and statistical parameters are presented in each figure legend.

Reporting Summary. Further information on research design is available in the Nature Research Reporting Summary linked to this article.

Data availability

All data in the present study are available within the article and its Supplementary files and from the corresponding author upon reasonable request. Source data are provided with this paper.

References

49. Yang, Z. et al. Restoring oxidant signaling suppresses proarthritogenic T cell effector functions in rheumatoid arthritis. *Sci. Transl. Med.* **8**, 331ra338 (2016).
50. Li, Y. et al. Deficient activity of the nuclease MRE11A induces T cell aging and promotes arthritogenic effector functions in patients with rheumatoid arthritis. *Immunity* **45**, 903–916 (2016).

Acknowledgements

This work was supported by the National Institutes of Health (grant nos. R01AR042527, R01AI108906, R01HL142068 and P01HL129941 to C.M.W. and nos. R01AI108891, R01AG045779, U19AI057266 and R01AI129191 to J.J.G.).

Author contributions

C.M.W., J.J.G. and B.W. conceived the project. B.W., T.V.Z., Z.H. and K.J. formally analyzed and investigated the data. K.J.W. and M.P.A. recruited the patients. C.M.W., J.J.G. and B.W. wrote the original manuscript. C.M.W. and J.J.G. supervised the study. C.M.W. and J.J.G. acquired the funds.

Competing interests

The authors declare no competing interests.

Additional information

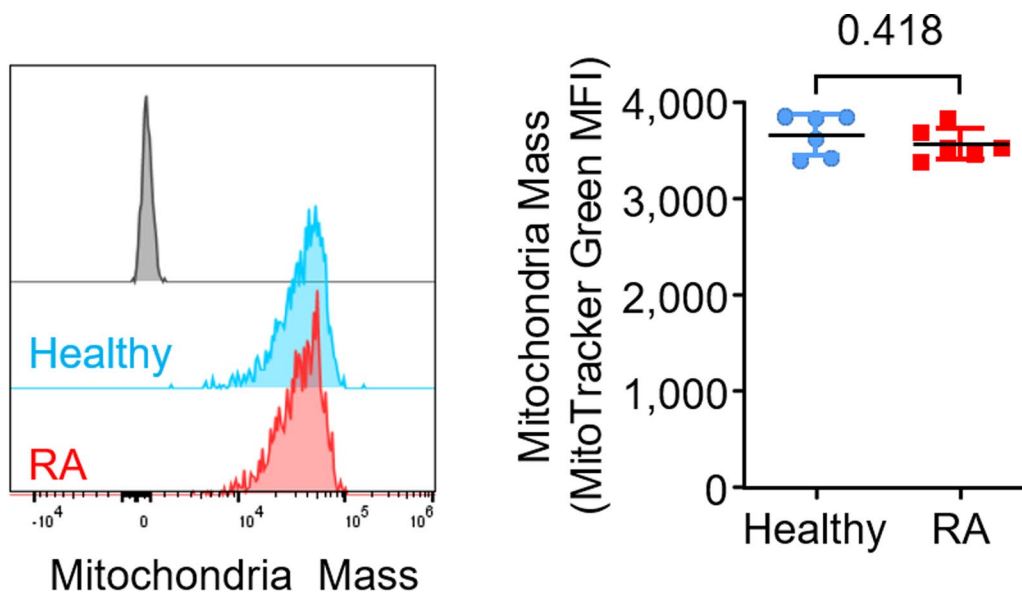
Extended data are available for this paper at <https://doi.org/10.1038/s41590-021-01065-2>.

Supplementary information The online version contains supplementary material available at <https://doi.org/10.1038/s41590-021-01065-2>.

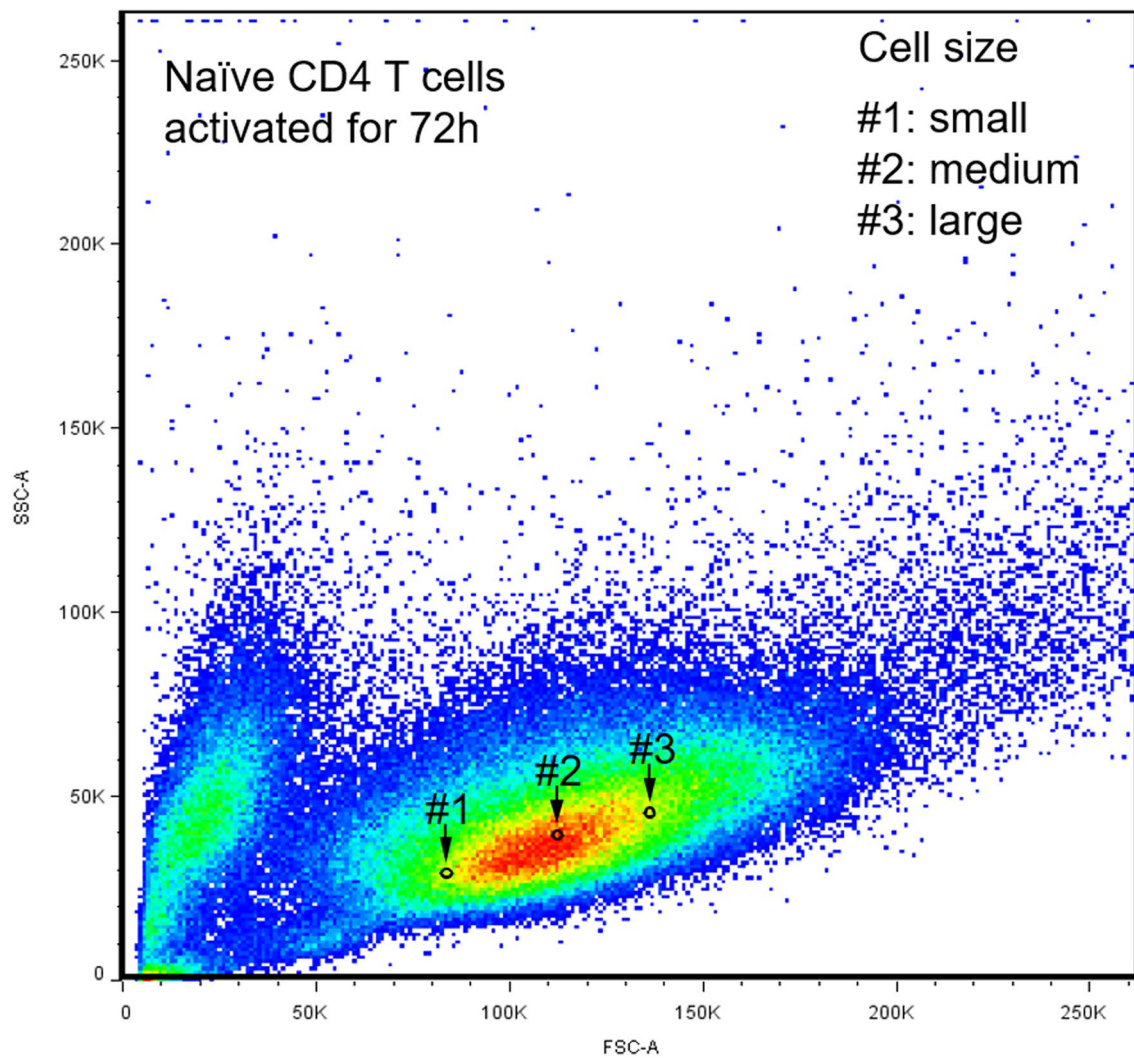
Correspondence and requests for materials should be addressed to Cornelia M. Weyand.

Peer review information *Nature Immunology* thanks Navdeep Chandel and George Tsokos for their contribution to the peer review of this work. N. Bernard was the primary editor on this article and managed its editorial process and peer review in collaboration with the rest of the editorial team. Peer review reports are available.

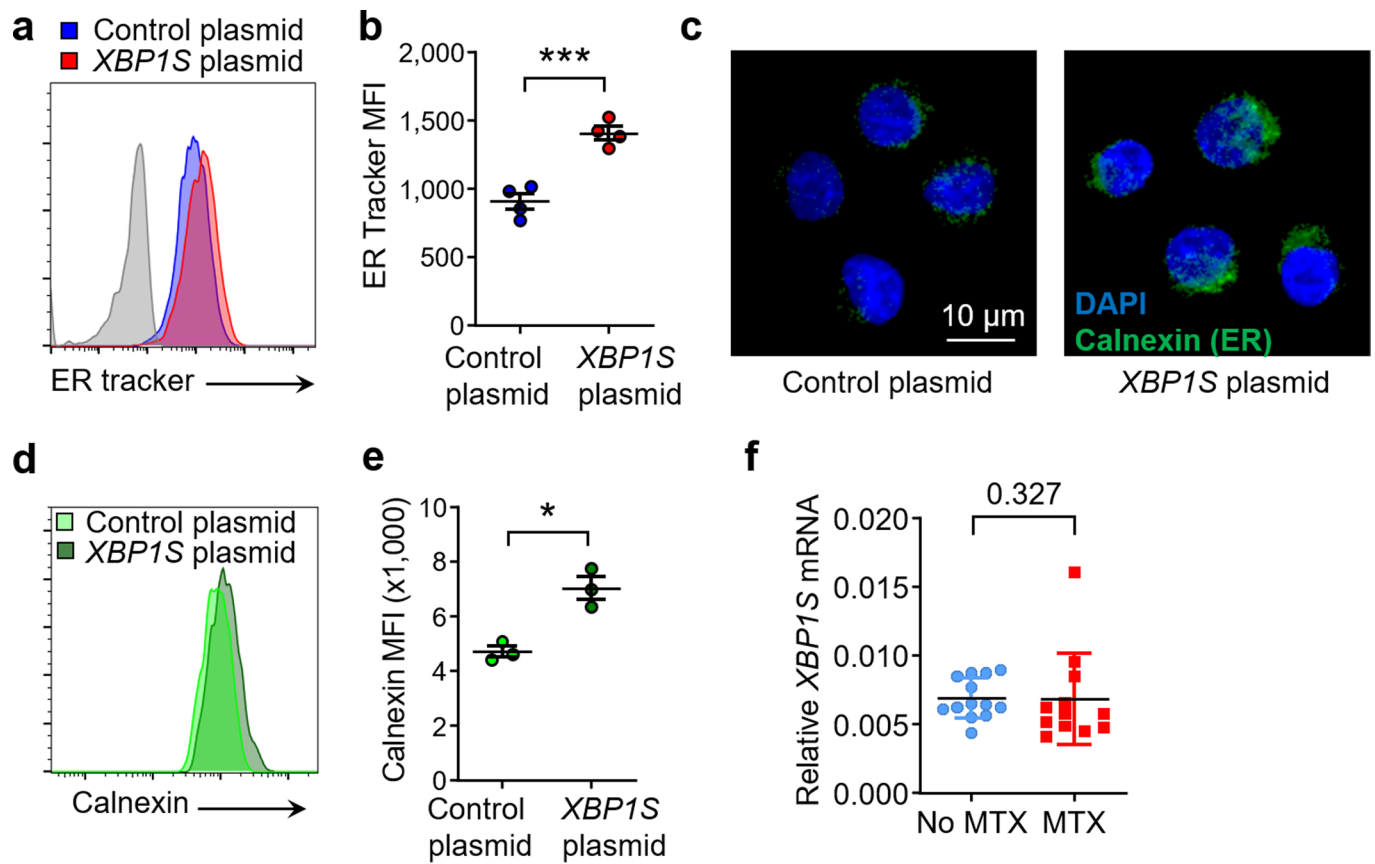
Reprints and permissions information is available at www.nature.com/reprints.



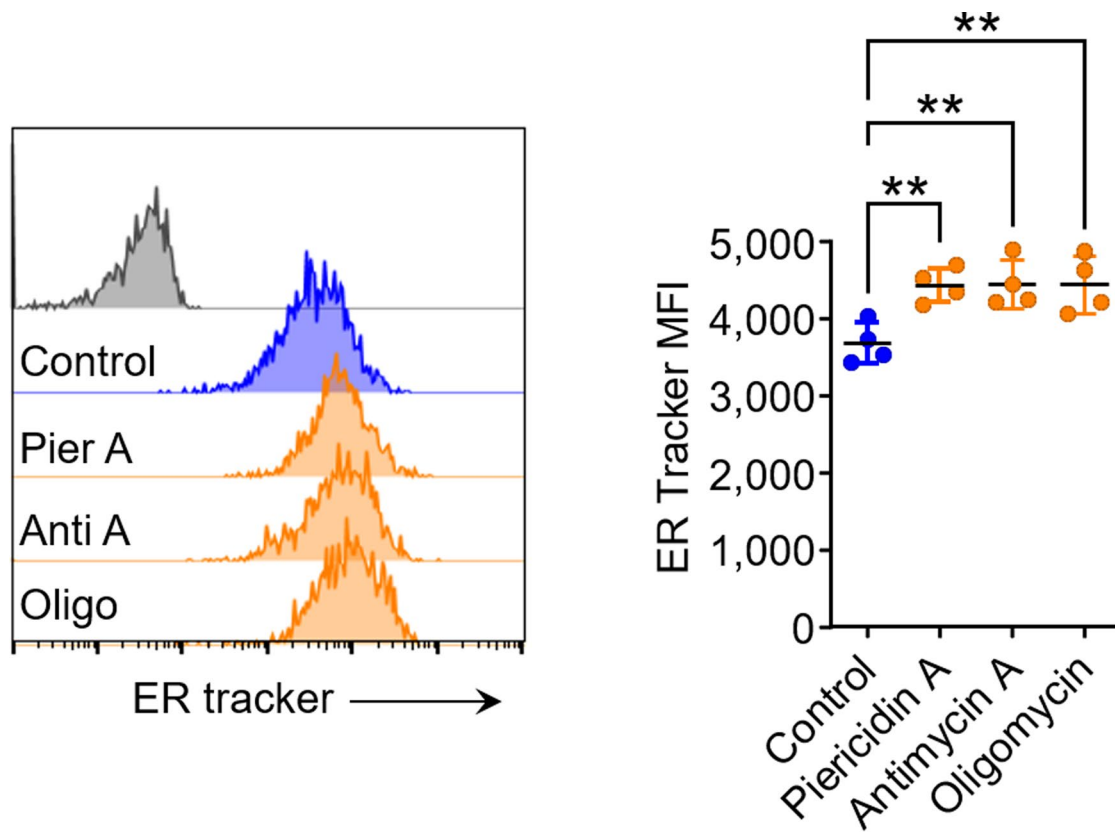
Extended Data Fig. 1 | Mitochondrial mass in healthy and RA T cells. CD4⁺CD45RA⁺ T cells were stimulated for 72 h. Flow cytometric quantification of mitochondria mass (MitoTrack Green MFI); n=6 healthy and 6 RA. Data are mean \pm SEM. Two-tailed unpaired Mann-Whitney-Wilcoxon rank test.



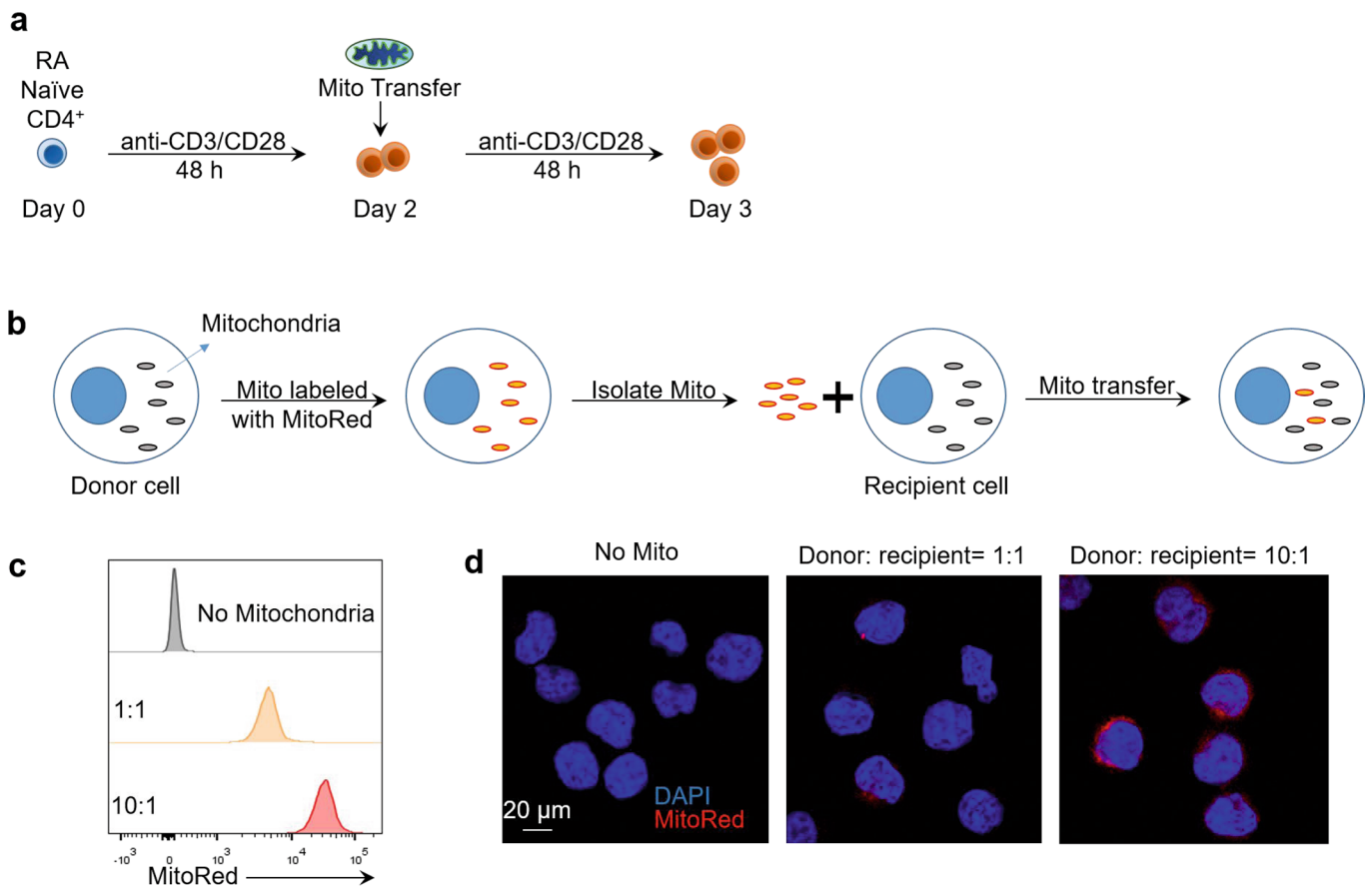
Extended Data Fig. 2 | Gating strategy to analyze ER and mitochondrial function on the single cell level. CD4⁺CD45RA⁺ T cells were stimulated for 72 h. ER biomass was determined with ER tracker and mitochondrial function was assessed with the mitochondrial membrane potential. Gate #1: small cellular size. Gate #2: medium cellular size. Gate #3: large cellular size.



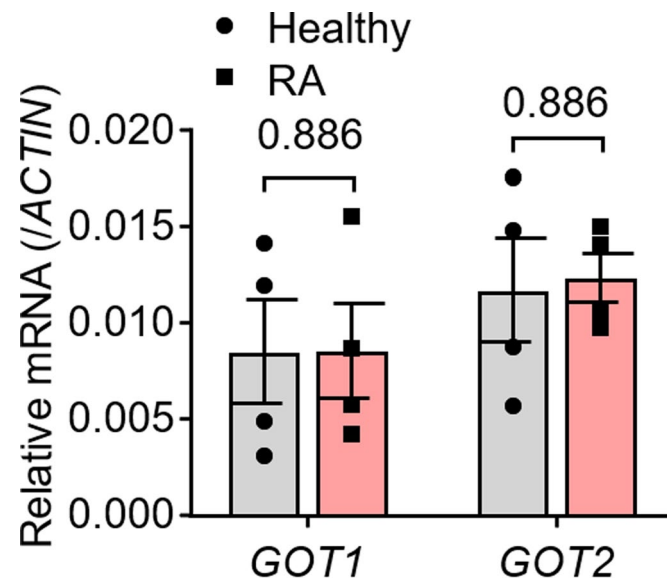
Extended Data Fig. 3 | XBP1S overexpression induces ER expansion. Naive CD4⁺ T cells were stimulated and transfected with control or XBP1S overexpression plasmid before the ER size was determined. **(a, b)** Flow cytometry for ER Tracker staining; $n=4$. **(c)** Confocal microscopy imaging of the ER protein calnexin. Scale bar, 10 μ m, $n=3$ independent experiments. **(d, e)** Flow cytometry for calnexin expression; $n=3$. **(f)** XBP1S expression in T cells from patients treated with or w/o Methotrexate (MTX) (MTX: $n=13$; w/o MTX: $n=12$). All data are mean \pm SEM. Two-tailed paired t test (b, e). Unpaired Mann-Whitney-Wilcoxon rank test (f). * $P < 0.05$, *** $P < 0.001$.



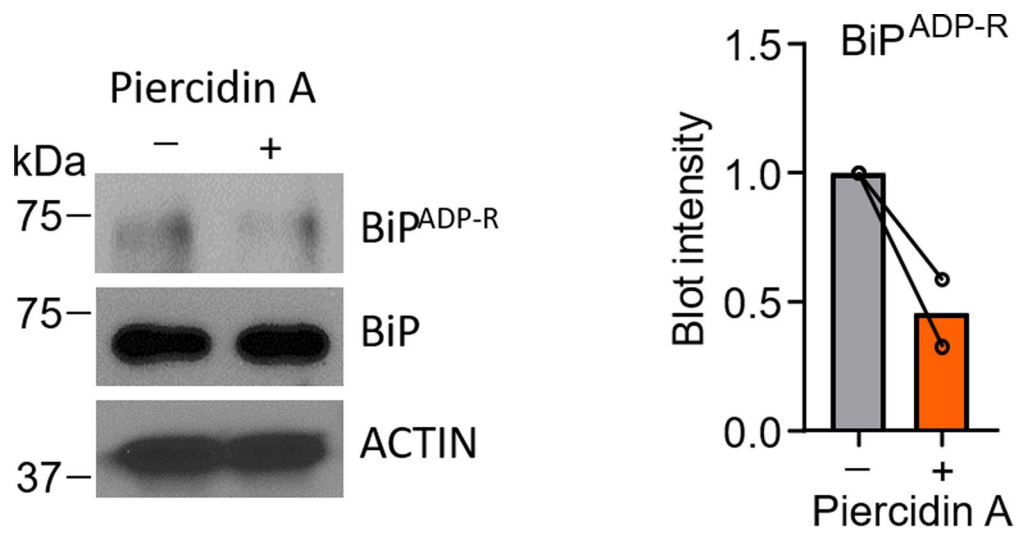
Extended Data Fig. 4 | Inhibitors of mitochondrial respiration promote ER expansion. Healthy naive CD4⁺ T cells were stimulated for 72 h in the presence of the mitochondrial respiration inhibitors Piericidin A (10 pM), Antimycin A (10 nM) or Oligomycin (1 nM). ER size was determined by flow cytometry measuring ER tracker (n = 4). Data are mean ± SEM. One-way ANOVA and post-ANOVA pair-wise two-group comparisons conducted with Tukey's method. **P < 0.01.



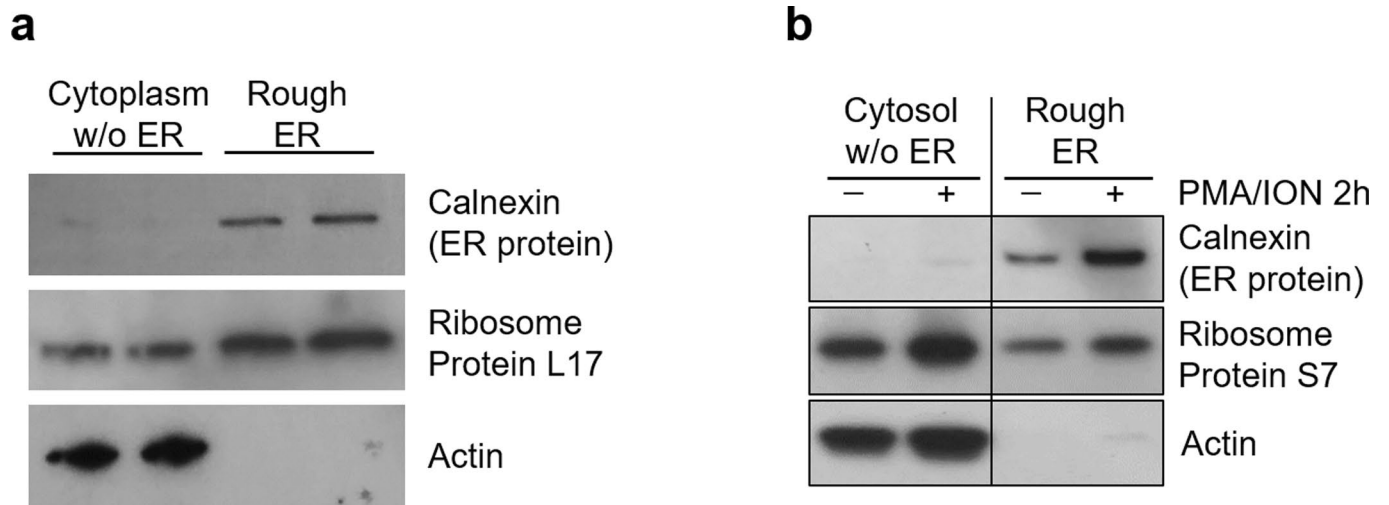
Extended Data Fig. 5 | Experimental scheme for mitochondria transfer. (a) Experimental scheme for mitochondria transfer into RA T cells. (b) Experimental scheme for mitochondria transfer in Jurkat T cells. Mitochondria were labeled with MitoTrackerRed and isolated, then transferred into recipient cells. (c) Flow cytometric analysis of MitoTracker Red intensity after mitochondria transfer. Ratio indicates donor cell number/recipient cell number. (d) Representative confocal imaging of exogenous mitochondria transferred into Jurkat T cells, $n=3$ independent experiments, scale bar, 20 μm .



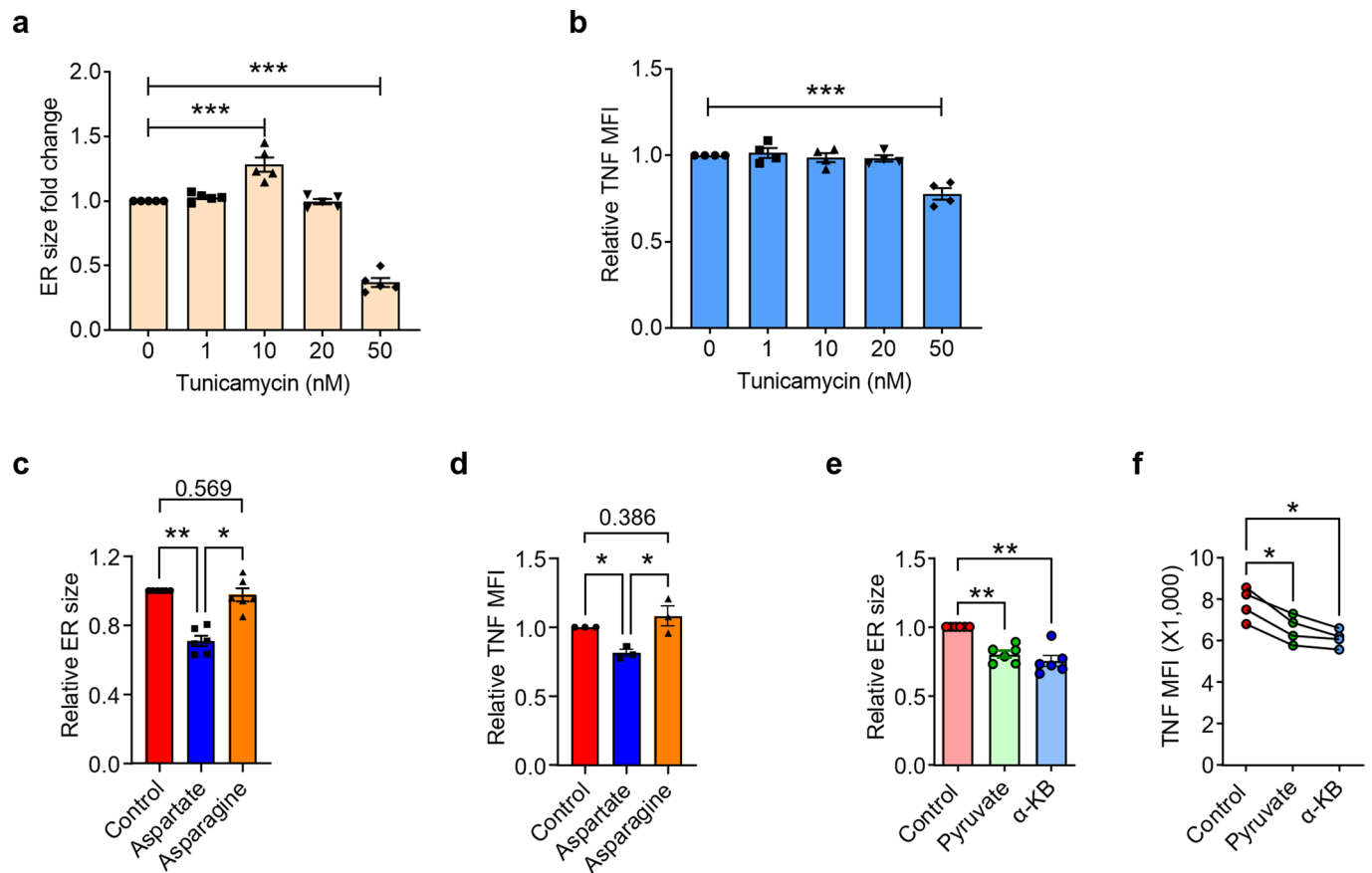
Extended Data Fig. 6 | Expression of GOT1 and GOT2 in healthy and RA T cells. Peripheral blood CD4⁺CD45RA⁺ T cells from patients with RA and age-matched healthy individuals were isolated and stimulated for 72 h. mRNA levels of *GOT1* and *GOT2* were determined by qPCR. n=4 in each group. All data are mean \pm SEM. Two-tailed unpaired Mann-Whitney-Wilcoxon rank test.



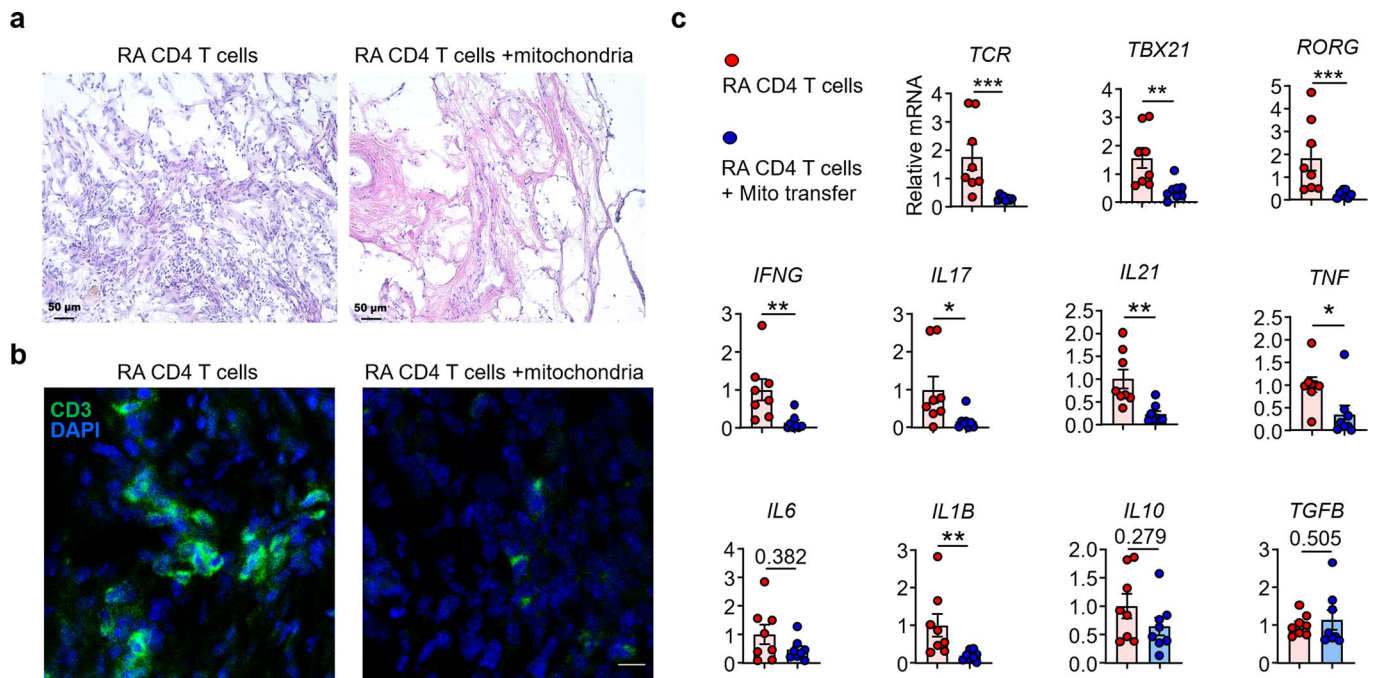
Extended Data Fig. 7 | Mitochondrial complex I inhibitor Piercidin A inhibits ADP-ribosylation of BiP. ADP-ribosylation of BiP in healthy CD4⁺ T cells treated with or w/o Piercidin A (10 pM) for 24 h. n=2.



Extended Data Fig. 8 | Isolation of Rough ER. (a) Naïve CD4⁺ T cells were purified from peripheral blood mononuclear cells and stimulated with anti-CD3/CD28 for 72 h. The rough ER was isolated by calcium precipitation and the isolate was immunoblotted for the ER protein calnexin, the ribosomal protein L17 and the cytoplasmic protein α -actin. (b) Healthy CD4⁺ T cells were activated with PMA/Ionomycin for 2 h before isolation of the rough ER and immunoblotting of the ER protein calnexin, the ribosomal protein S7 and the cytosolic protein β -actin.



Extended Data Fig. 9 | Effects of Tunicamycin, aspartate, asparagine, pyruvate, and α -ketobutyrate on ER size and TNF production. Naïve CD4⁺ T cells were purified from PBMCs and stimulated with anti-CD3/CD28 beads for 72 h in the presence of the indicated molecules. ER size quantified by MFI of ER tracker staining and TNF production measured by intracellular staining of TNF after PMA/ION stimulation for 2 h in the presence of the secretion inhibitor BFA. **(a)** Fold change of ER size after Tunicamycin treatment compared to the control group, $n = 6$. **(b)** Fold change of TNF production after Tunicamycin treatment compared to the control group, $n = 4$. **(c)** ER size change after Aspartate (1 mM) or Asparagine (1 mM) treatment, $n = 6$. **(d)** TNF production after aspartate and asparagine treatment, $n = 3$. **(e)** ER size change after pyruvate (1 mM) or α -KB (1 mM) treatment, $n = 6$. **(f)** TNF production after pyruvate or α -KB treatment, $n = 4$. All data are mean \pm SEM, one-way ANOVA and post-ANOVA pair-wise two-group comparisons conducted with Tukey's method. * $P < 0.05$, ** $P < 0.01$, *** $P < 0.001$.



Extended Data Fig. 10 | Mitochondria transfer into CD4+ T cells protects synovial tissue from inflammation. Mitochondria were isolated from healthy T cells and transferred into RA CD4⁺ T cells prior to their adoptive transfer into synovium-NSG chimeras. Explanted synovial grafts were analyzed by immunohistochemical staining and tissue transcriptomics (RT-PCR). 8 tissues in each group. **(a)** H&E staining of synovial tissue sections. Scale bar; 50 μm. **(b)** Immunofluorescence staining for CD3⁺ T cells in synovial infiltrates. Representative images. Scale bar; 10 μm. **(c)** Gene expression profiling (RT-PCR) of *TRB*, *TBET*, *RORG* and other key inflammatory markers (n=8). All data are mean ± SEM. Two-tailed unpaired Mann-Whitney-Wilcoxon rank test. *P < 0.05, **P < 0.01, ***P < 0.001.

Reporting Summary

Nature Research wishes to improve the reproducibility of the work that we publish. This form provides structure for consistency and transparency in reporting. For further information on Nature Research policies, see our [Editorial Policies](#) and the [Editorial Policy Checklist](#).

Statistics

For all statistical analyses, confirm that the following items are present in the figure legend, table legend, main text, or Methods section.

n/a Confirmed

- The exact sample size (n) for each experimental group/condition, given as a discrete number and unit of measurement
- A statement on whether measurements were taken from distinct samples or whether the same sample was measured repeatedly
- The statistical test(s) used AND whether they are one- or two-sided
Only common tests should be described solely by name; describe more complex techniques in the Methods section.
- A description of all covariates tested
- A description of any assumptions or corrections, such as tests of normality and adjustment for multiple comparisons
- A full description of the statistical parameters including central tendency (e.g. means) or other basic estimates (e.g. regression coefficient) AND variation (e.g. standard deviation) or associated estimates of uncertainty (e.g. confidence intervals)
- For null hypothesis testing, the test statistic (e.g. F , t , r) with confidence intervals, effect sizes, degrees of freedom and P value noted
Give P values as exact values whenever suitable.
- For Bayesian analysis, information on the choice of priors and Markov chain Monte Carlo settings
- For hierarchical and complex designs, identification of the appropriate level for tests and full reporting of outcomes
- Estimates of effect sizes (e.g. Cohen's d , Pearson's r), indicating how they were calculated

Our web collection on [statistics for biologists](#) contains articles on many of the points above.

Software and code

Policy information about [availability of computer code](#)

Data collection

Data analysis

For manuscripts utilizing custom algorithms or software that are central to the research but not yet described in published literature, software must be made available to editors and reviewers. We strongly encourage code deposition in a community repository (e.g. GitHub). See the Nature Research [guidelines for submitting code & software](#) for further information.

Data

Policy information about [availability of data](#)

All manuscripts must include a [data availability statement](#). This statement should provide the following information, where applicable:

- Accession codes, unique identifiers, or web links for publicly available datasets
- A list of figures that have associated raw data
- A description of any restrictions on data availability

All data in this study are available within the paper, source data are provided with this paper. Any other relevant data are available from the corresponding author upon reasonable request.

Field-specific reporting

Please select the one below that is the best fit for your research. If you are not sure, read the appropriate sections before making your selection.

Life sciences Behavioural & social sciences Ecological, evolutionary & environmental sciences

For a reference copy of the document with all sections, see [nature.com/documents/nr-reporting-summary-flat.pdf](https://www.nature.com/documents/nr-reporting-summary-flat.pdf)

Life sciences study design

All studies must disclose on these points even when the disclosure is negative.

Sample size	No sample size calculation was performed. In vivo experiments were performed at least with 8 synovial tissues. All in vitro experiments were repeated at with two independent biological replicates.
Data exclusions	No data was excluded.
Replication	All experiments were repeated by independent experiments at least twice, and all attempts at replication were successful.
Randomization	PBMCs from patients were randomly used in every experiments. For in vivo study, experimental mice were randomized to different groups.
Blinding	Blinded data collection and analysis was applied to all data.

Reporting for specific materials, systems and methods

We require information from authors about some types of materials, experimental systems and methods used in many studies. Here, indicate whether each material, system or method listed is relevant to your study. If you are not sure if a list item applies to your research, read the appropriate section before selecting a response.

Materials & experimental systems

Methods

n/a	Involved in the study	n/a	Involved in the study
<input type="checkbox"/>	<input checked="" type="checkbox"/> Antibodies	<input checked="" type="checkbox"/>	<input type="checkbox"/> ChIP-seq
<input type="checkbox"/>	<input checked="" type="checkbox"/> Eukaryotic cell lines	<input type="checkbox"/>	<input checked="" type="checkbox"/> Flow cytometry
<input checked="" type="checkbox"/>	<input type="checkbox"/> Palaeontology and archaeology	<input checked="" type="checkbox"/>	<input type="checkbox"/> MRI-based neuroimaging
<input type="checkbox"/>	<input checked="" type="checkbox"/> Animals and other organisms		
<input type="checkbox"/>	<input checked="" type="checkbox"/> Human research participants		
<input checked="" type="checkbox"/>	<input type="checkbox"/> Clinical data		
<input checked="" type="checkbox"/>	<input type="checkbox"/> Dual use research of concern		

Antibodies

Antibodies used

Anti-human PDI Monoclonal Antibody Thermo Fisher Scientific MA3-019; Immunofluorescence (IF), 1:200
 Anti-human Calnexin Monoclonal Antibody Cell Signalling Technology 2679S; IF, 1:200; Western blot, 1:2000
 Anti-human CD3 Monoclonal Antibody Dako M725401-2; IF, 1:200
 Anti-human Interferon gamma polyclonal antibody Abcam ab25101; IF, 1:200
 Anti-human BIP Monoclonal Antibody Santa Cruz Biotechnology sc-13539; Western blot, 1:1000; Immunoprecipitation(IP), 1ug/0.5mL
 Anti-human Poly/Mono-ADP Ribose Monoclonal Antibody Cell Signalling Technology 83732S; Western blot, 1:1000
 Anti-human IRE1 α Monoclonal Antibody Cell Signalling Technology 3294S; Western blot, 1:1000
 Anti-human Ribosomal Protein L17 Monoclonal Antibody Santa Cruz Biotechnology sc-515904; Western blot, 1:1000
 Anti-human Ribosomal Protein S7 Monoclonal Antibody Santa Cruz Biotechnology sc-377317; Western blot, 1:1000
 Anti-human TNF alpha Monoclonal Antibody Abcam ab1793; IF, 1:200
 Anti-human β -Actin Monoclonal Antibody Cell Signalling Technology 3700S; Western blot, 1:5000
 Normal rat IgG Santa Cruz Biotechnology sc-2026; IP, 1ug/0.5mL
 Goat anti-Rat IgG-HRP Cell Signalling Technology 7077S; Western blot, 1:5000
 Goat anti-Rabbit IgG-HRP Cell Signalling Technology 7074S; Western blot, 1:5000
 Goat anti-Mouse IgG-HRP Abcam ab6789; Western blot, 1:5000
 Alexa Fluor 488 Goat Anti-mouse IgG Abcam ab96879; IF, 1:200
 Alexa Fluor 594 Goat Anti-mouse IgG Thermo Fisher Scientific A-11032; IF, 1:200
 Alexa Fluor 488 Goat Anti-Rabbit IgG Thermo Fisher Scientific A-11034; IF, 1:200
 Alexa Fluor 594 Goat Anti-Rabbit IgG Thermo Fisher Scientific A-11012; IF, 1:200
 PE/Cyanine7 Anti-human CD45 Antibody BioLegend 368532; Flow cytometry, 1:200
 Brilliant Violet 421™ Anti-human CD3 Antibody BioLegend 344834; Flow cytometry, 1:200
 APC anti-human CD163 Antibody BioLegend 333610; Flow cytometry, 1:200
 Brilliant Violet 785™ anti-human CD19 Antibody BioLegend 302239; Flow cytometry, 1:200

FITC anti-human TNF- α Antibody BioLegend 502906; Flow cytometry, 1:200
PE anti-human TNF- α Antibody BD Pharm 554513; Flow cytometry, 1:200

Validation

All antibodies are commercial clones that have been verified by the suppliers. Please refer to the data sheet from the vendor's website for technical info by searching the catalog number provided.

Eukaryotic cell lines

Policy information about [cell lines](#)

Cell line source(s)

Jurkat T cell line, from ATCC

Authentication

Jurkat cell line was not validated.

Mycoplasma contamination

The cell line is not tested for mycoplasma contamination.

Commonly misidentified lines
(See [ICLAC](#) register)

The study didn't involve misidentified lines.

Animals and other organisms

Policy information about [studies involving animals](#); [ARRIVE guidelines](#) recommended for reporting animal research

Laboratory animals

NOD.Cg-Prkdcscidll2rgtm1Wjl/SzJ (NSG) mice were maintained and bred under specific pathogen-free conditions on a 12/12 h light/dark cycle at 20-22°C with free access to water and food. Animal housing facilities were monitored for infection with specific pathogens every 6 weeks and the health status of all animals was checked on a daily basis. Both male and female mice were randomly used at 8-12 weeks of age.

Wild animals

The study did not involve wild animals.

Field-collected samples

The study did not involve field-collected samples

Ethics oversight

Administrative Panel on Laboratory Animal Care (APLAC), Stanford University; Mayo Clinic Institutional Animal Care and Use Committee

Note that full information on the approval of the study protocol must also be provided in the manuscript.

Human research participants

Policy information about [studies involving human research participants](#)

Population characteristics

Patients with RA were 53.6 ± 16.1 years old, 76.0% female and 21.7% untreated, 9.2% are DMARD naive, 15.8% on corticosteroids, 35.8% on methotrexate, 17.5% on hydroxychloroquine, 18.3% on TNF inhibitors, and 41.7% on other DMARDs. Patients with PsA were 55.7 ± 12.2 years old, 46.7% female and 13.3% untreated, 13.3% are DMARD naive, 4.7% on corticosteroids, 53.3% on methotrexate, 20.0% on TNF inhibitors, and 40.0% on other DMARDs.

Recruitment

Patients with a diagnosis of RA (n=120) who fulfilled the diagnostic criteria for RA, positive for rheumatoid factor and/or anti-cyclic citrullinated peptide antibodies were recruited into the study. Patients with a diagnosis of psoriatic arthritis (PsA, n=15) served as control disease group. Individuals with cancer, uncontrolled medical disease or any other inflammatory syndrome were excluded. Age-matched healthy donors without a personal or family history of cancer or autoimmune disease were enrolled as healthy controls.

Ethics oversight

Institutional Review Board (IRB) Stanford; Institutional Review Board (IRB) Mayo Clinic

Note that full information on the approval of the study protocol must also be provided in the manuscript.

Flow Cytometry

Plots

Confirm that:

- The axis labels state the marker and fluorochrome used (e.g. CD4-FITC).
- The axis scales are clearly visible. Include numbers along axes only for bottom left plot of group (a 'group' is an analysis of identical markers).
- All plots are contour plots with outliers or pseudocolor plots.
- A numerical value for number of cells or percentage (with statistics) is provided.

Methodology

Sample preparation

Cells examined in this study were derived from peripheral blood mononuclear cells (PBMC) that were purified from peripheral blood by density gradient centrifugation with Lymphoprep (STEMCELL Technologies). Naïve CD4⁺ CD45RA⁺ T cells

were purified from fresh PBMCs using an EasySep™ Human naïve CD4 T Cell Enrichment Kit (STEMCELL Technologies, #17555).

Instrument

BD LSRFortessa flow cytometer or CYTEK NL-3000

Software

FlowJo v10.7.2 (Tree Star Inc.)

Cell population abundance

The purity of cell population was consistently > 95% determined by flow cytometry.

Gating strategy

Fluorescence minus one (FMO) was used to define the positive and negative populations for all experiments.

Tick this box to confirm that a figure exemplifying the gating strategy is provided in the Supplementary Information.